UC San Diego
UC San Diego Previously Published Works

Title
Estimation of Thalamocortical and Intracortical Network Models from Joint Thalamic Single-Electrode and Cortical Laminar-Electrode Recordings in the Rat Barrel System

Permalink
https://escholarship.org/uc/item/4r53q5tk

Journal
PLOS Computational Biology, 5(3)

ISSN
1553-734X

Authors
Blomquist, Patrick
Devor, Anna
Indahl, Ulf G
et al.

Publication Date
2009-03-01

DOI
10.1371/journal.pcbi.1000328

Peer reviewed

Estimation of Thalamocortical and Intracortical Network Models from Joint Thalamic Single-Electrode and Cortical Laminar-Electrode Recordings in the Rat Barrel System

Patrick Blomquist[1], Anna Devor[2,3], Ulf G. Indahl[1], Istvan Ulbert[4,5], Gaute T. Einevoll[1]*, Anders M. Dale[3]

1 Department of Mathematical Sciences and Technology and Center for Integrative Genetics, Norwegian University of Life Sciences, Ås, Norway, 2 Athinoula A. Martinos Center, Massachusetts General Hospital, Charlestown, Massachusetts, United States of America, 3 Departments of Radiology and Neurosciences, University of California San Diego, La Jolla, California, United States of America, 4 Institute for Psychology of the Hungarian Academy of Sciences, Budapest, Hungary, 5 Peter Pazmany Catholic University, Department of Information Technology, Budapest, Hungary

Abstract

A new method is presented for extraction of population firing-rate models for both thalamocortical and intracortical signal transfer based on stimulus-evoked data from simultaneous thalamic single-electrode and cortical recordings using linear (laminar) multielectrodes in the rat barrel system. Time-dependent population firing rates for granular (layer 4), supragranular (layer 2/3), and infragranular (layer 5) populations in a barrel column and the thalamic population in the homologous barreloid are extracted from the high-frequency portion (multi-unit activity; MUA) of the recorded extracellular signals. These extracted firing rates are in turn used to identify population firing-rate models formulated as integral equations with exponentially decaying coupling kernels, allowing for straightforward transformation to the more common firing-rate formulation in terms of differential equations. Optimal model structures and model parameters are identified by minimizing the deviation between model firing rates and the experimentally extracted population firing rates. For the thalamocortical transfer, the experimental data favor a model with fast feedforward excitation from thalamus to the layer-4 laminar population combined with a slower inhibitory process due to feedforward and/or recurrent connections and mixed linear-parabolic activation functions. The extracted firing rates of the various cortical laminar populations are found to exhibit strong temporal correlations for the present experimental paradigm, and simple feedforward population firing-rate models combined with linear or mixed linear-parabolic activation function are found to provide excellent fits to the data. The identified thalamocortical and intracortical network models are thus found to be qualitatively very different. While the thalamocortical circuit is optimally stimulated by rapid changes in the thalamic firing rate, the intracortical circuits are low-pass and respond most strongly to slowly varying inputs from the cortical layer-4 population.

Introduction

Following pioneering work in the 1970s by, e.g., Wilson and Cowan [1] and Amari [2] a substantial effort has been put into the investigation of neural network models, particularly in the form of *firing-rate* or *neural field* models [3]. Some firing-rate network models, in particular for the early visual system ([4], Ch.2), have been developed to account for particular physiological data. However, for strongly interconnected cortical networks, few mechanistic network models directly accounting for specific neurobiological data have been identified. Instead most work has been done on generic network models and has focused on the investigation of generic features, such as the generation and stability of localized bumps, oscillatory patterns, traveling waves and pulses and other coherent structures, for reviews see Ermentrout [5] or Coombes [6].

We here (1) present a new method for identification of *specific* population firing-rate network models from extracellular recordings, (2) apply the method to extract network models for thalamocortical and intracortical signal processing based on stimulus-evoked data from simultaneous single-electrode and multielectrode extracellular recordings in the rat somatosensory (barrel) system, and (3) analyze and interpret the identified firing-rate models using techniques from dynamical systems analysis. Our study reveals large differences in the transfer function between thalamus (VPM) and layer 4 of the barrel column, compared to that between cortical layers, and thus sheds direct light on how whisker stimuli is encoded in population firing-activity in the somatosensory system.

The derivation of biologically realistic, cortical neural-network models has generally been hampered by the lack of relevant experimental data to constrain and test the models. Single electrodes can generally only measure the firing activity of individual neurons, not the joint activity of populations of cells typically predicted by population firing-rate models. Kyriazi and Simons [7] and Pinto et al. [8,9] thus developed models for the somatosensory thalamocortical signal transformation based on pooled data from single-unit recordings from numerous animals.

Author summary

Many of the salient features of individual cortical neurons appear well understood, and several mathematical models describing their physiological properties have been developed. The present understanding of the highly interconnected cortical neural networks is much more limited. Lack of relevant experimental data has in general prevented the construction and rigorous testing of biologically realistic cortical network models. Here we present a new method for extracting such models. In particular we estimate specific mathematical models describing the sensory activation of thalamic and cortical neuronal populations in the rat whisker system from joint recordings of extracellular potentials in thalamus and cortex. The mathematical models are formulated in terms of average firing rates of a thalamic population and a set of laminarly organized cortical populations, the latter extracted from data from linear (laminar) multielectrodes inserted perpendicularly through cortex. The identified models describing the signal processing from thalamus to cortex are found to be qualitatively very different from the models describing the processing between cortical populations; while the thalamocortical circuit is optimally stimulated by rapid changes in the thalamic firing rate, the intracortical circuits respond most strongly to slowly varying inputs.

By contrast, multielectrode arrays provide a convenient and powerful technology for obtaining simultaneous recordings from all layers of the cerebral cortex, at one or more cortical locations [10]. The signal at each low-impedance electrode contact represents a weighted sum of the potential generated by synaptic currents and action potentials of neurons within a radius of a few hundred micrometers of the contact, where the weighting factors depend on the shape and position of the neurons, as well as the electrical properties of the conductive medium [11–13].

In the present paper we describe a new method for extraction of population firing-rate models for both thalamocortical and intracortical transfer on the basis of data from simultaneous thalamic single-electrode and cortical recordings using linear (laminar) multielectrodes in the rat barrel system. With so called *laminar population analysis (LPA)* Einevoll et al. [11] jointly modeled the low-frequency (*local field potentials; LFP*) and high-frequency (*multi-unit activity; MUA*) parts of such stimulus-evoked laminar electrode data to estimate (1) the laminar organization of cortical populations in a barrel column, (2) time-dependent population firing rates, and (3) the LFP signatures following firing in a particular population. These 'postfiring' population LFP signatures were further used to estimate the synaptic connection patterns between the various populations using both *current source density (CSD)* estimation techniques and a new LFP template-fitting technique [11].

Here we use the stimulus-evoked time-dependent firing rates for the cortical populations estimated using LPA, in combination with single-electrode recordings of the firing activity in the homologous barreloid in VPM, to identify population firing-rate *models*. The models are formulated as nonlinear Volterra integral equations with exponentially decaying coupling kernels allowing for a mapping of the systems to sets of differential equations, the more common mathematical representation of firing-rate models [5,14].

The population responses were found to increase monotonically both with increasing amplitude and velocity of the whisker flick [11,15,16]. A stimulus set varying both the whisker-flicking amplitude and the rise time was found to provide a rich variety

of thalamic and cortical responses and thus to be well suited for distinguishing between candidate models. The optimal model structure and corresponding model parameters are estimated by minimizing the mean-square deviation between the population firing rates predicted by the models and the experimentally extracted population firing rates.

A first focus is on the estimation of mathematical models for the signal transfer between thalamus (VPM) and the layer-4 population, the population receiving the dominant thalamic input. For this thalamocortical transfer our experimental data favors a model with (1) fast feedforward excitation, (2) a slower predominantly inhibitory process mediated by a combination of recurrent (within layer 4) and feedforward interactions (from thalamus), and (3) a mixed linear-parabolic activation function. The identified thalamo-cortical circuits are seen to have a band-pass property, and in the frequency domain the largest responses for the layer-4 population is obtained for thalamic firing rates with frequencies around twenty Hz.

Very different population firing-rate models are identified for the intracortical circuits, i.e., the spread of population activity from layer 4 to supragranular (layer 2/3) and infragranular (layer 5) layers. For the present experimental paradigm the extracted firing rates of the various cortical laminar populations are found to exhibit strong temporal correlations and simple feedforward models with linear or mixed linear-parabolic activation function are found to account excellently for the data. The functional properties of the identified thalamocortical and intracortical network models are thus qualitatively very different: while the thalamocortical circuit is optimally stimulated by rapid changes in the thalamic firing rate, the intracortical circuits are low-pass and respond strongest to slowly varying inputs.

Preliminary results from this project were presented earlier in poster format [17].

Results

Here we illustrate our approach by first showing results from one of the six experimental data sets considered, and next show the thalamic and cortical laminar population responses extracted from these experimental data. Further, we outline the general form of the neural population models we explore to account for these population firing. We then go on to test specific candidate *thalamocortical* models against the experimentally observed population responses in layer 4 using the experimental thalamic response as driving input to the model. The identified thalamocortical models found by minimizing the deviation between model predictions and experimental population firing rates are further analyzed and explored using tools from dynamical system analysis. Finally, we correspondingly examine how the experimentally measured laminar population responses in layer 2/3 and layer 5, respectively, can be explained by *intracortical* network models with the experimental layer-4 population responses as input.

Experimental data and extracted population firing rates

In Figure 1 we show trial-averaged *multi-unit activity (MUA)* data for one of six experiments, labeled 'experiment 1', from stimulus onset, i.e., onset of whisker-flick, until 100 ms after. This is the time window of data used in the further analysis. Color plots depict the laminar-electrode recordings while the line plots below show the corresponding trial-averaged thalamic recordings. Results for 9 of 27 stimulus conditions are shown, corresponding to three different stimulus rise times ($t9,t5,t1$) for three different stimulus amplitudes ($a1,a2,a3$). Neurons in the barrel cortex are sensitive to both stimulus amplitude and stimulus velocity (and thus stimulus rise time) [11,15,16], and we found that a set of stimuli
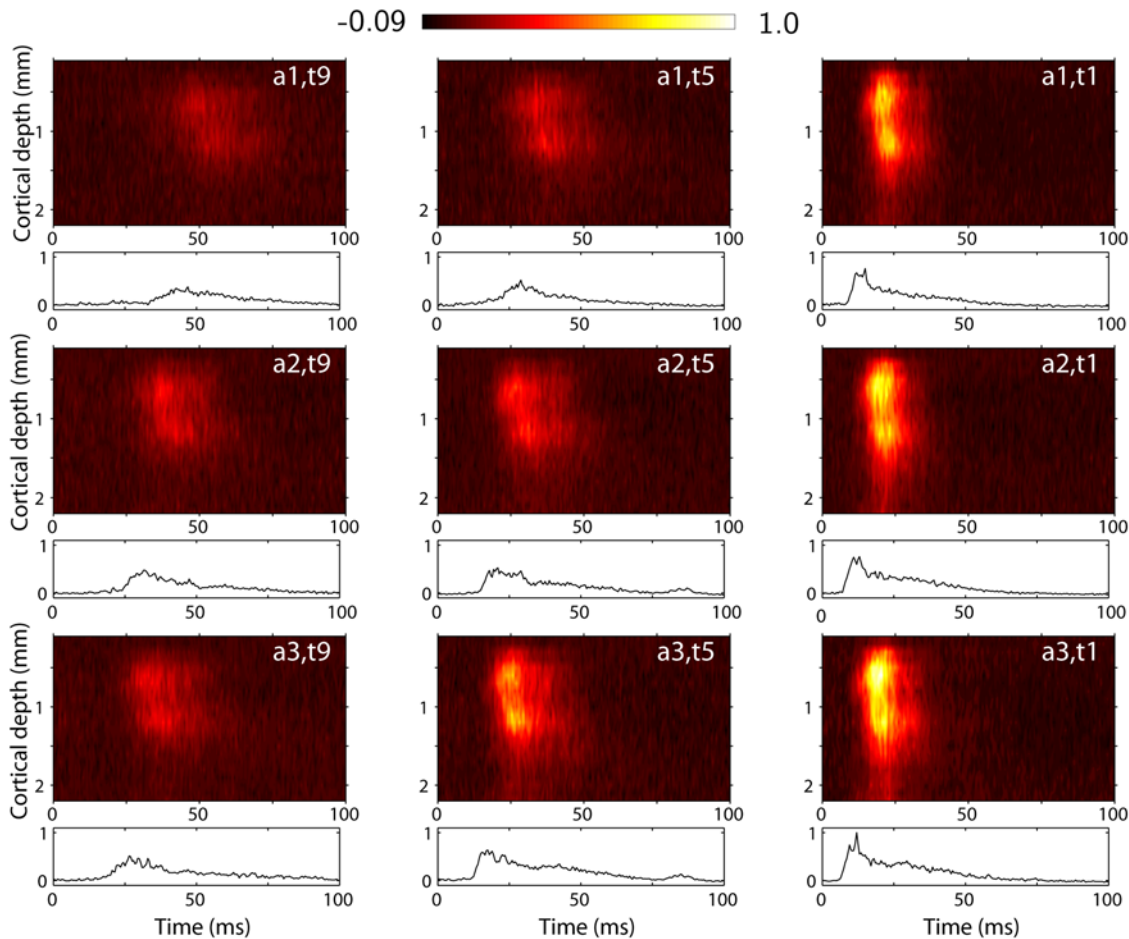
Figure 1. Example experimental data. Trial-averaged experimental data for experiment 1 for 9 out of 27 applied stimulus conditions for three different amplitudes (rows) and three different rise times (columns). Contour plots show depth profile of MUA as recorded by the laminar electrode, normalized to its largest value over the 22 electrode traces and 27 stimulus condition. Line plots below show the corresponding thalamic MUA recorded by a single electrode, normalized to the largest value over the 27 stimulus conditions.
doi:10.1371/journal.pcbi.1000328.g001

varying both the amplitude and rise time provide a rich variety of responses suitable for the present study.

Fig. 2 shows the estimated thalamic $\left(r_T^x(t)\right)$ and cortical $\left(r_n^x(t), n=2/3,4,5\right)$ population firing rates extracted from the data in Fig. 1 (procedure described in Materials and Methods). The estimated thalamic population firing rate is essentially just a low-pass filtered version of the thalamic MUA. The cortical population firing rates have been estimated by a method from the recently developed *laminar population analysis (LPA)* [11] where the MUA from the full set of electrode contacts on the laminar electrode is modeled as a sum over contributions from a set of laminar populations, cf. Eqs. (16–17). In the present case four cortical populations are assumed in this firing-rate extraction scheme [11], but the figure only shows results for the three cortical populations considered in this study, namely the layer 2/3 $(n=2/3)$, layer 4 $(n=4)$, and layer 5 $(n=5)$ populations. A deeper laminar population was also identified, but it was left out of the present analysis since predictions related to the postsynaptic LFP-profiles from this particular population were found to vary between different experiments, thus questioning its proper identification [11].

Form of thalamocortical model

We first focus on the signal transfer between thalamus and the dominant input layer of the barrel column, namely layer 4.

Specifically we seek a mathematical model predicting the layer-4 population firing rate $r_4^x(t)$ for all 27 stimulus conditions (of which nine are depicted in Fig. 2) given the corresponding thalamic population firing $r_T^x(t)$ as model input.

The stimulus-evoked dynamics of the excitatory and inhibitory neurons in layer 4 of the barrel column is complex. The excitatory neurons receive both feedforward excitation from thalamic neurons and recurrent excitation from other layer 4 excitatory cells [9,18–20]. In addition, the excitatory cells are inhibited by layer-4 interneurons [21]. These interneurons in turn receive feedforward excitation from thalamus [22–24] and recurrent inputs from other layer-4 neurons [9,21].

For mathematical convenience and conceptual simplicity we choose to formulate the population firing-rate model as Volterra integral equations [5,14]. In our so called *full thalamocortical* model where all the abovementioned feedforward and recurrent connections are included, we then have

$$r_4(t) = F_4\big(\big[(\beta_{Ef}h_{Ef} - \beta_{If}h_{If}) * r_T^x\big](t) + \big[(\beta_{Er}h_{Er} - \beta_{Ir}h_{Ir}) * r_4\big](t)\big) \tag{1}$$

Here the $h(t)$ are *temporal coupling kernels*, and $[h * r](t)$ is a *temporal convolution* between the temporal kernel $h(t)$ and the population
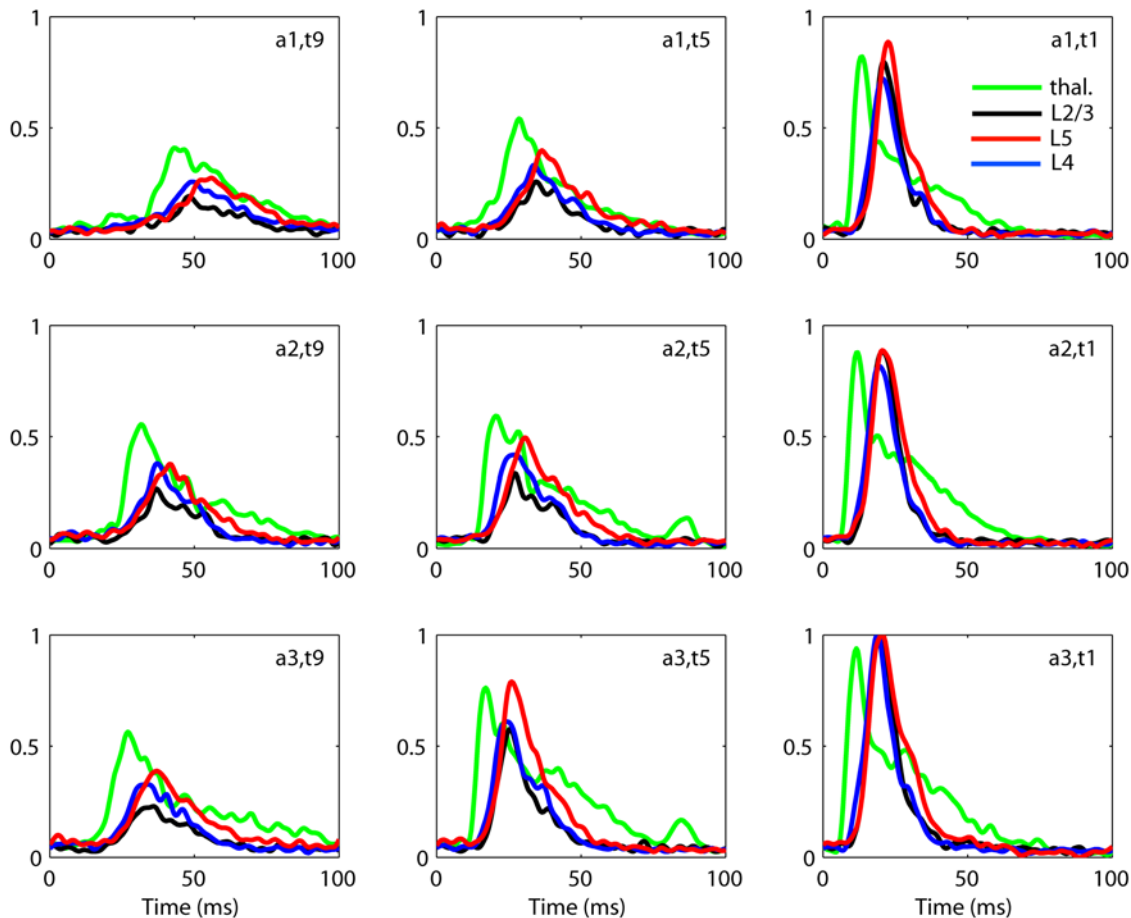
Figure 2. Example extracted population firing rates. Extracted population firing rates for experiment 1 for 9 out of 27 applied stimulus conditions. Green: thalamus. Black: layer 2/3. Blue: layer 4. Red: layer 5. Note that the extracted firing rates are normalized so that the maximum response over all stimulus conditions is unity. For layer 2/3, layer 4 and layer 5 this occurs for the stimulus (*a3,t1*) shown in the figure. For the thalamic rate it occurs for stimulus (*a3,t2*), not shown in the figure.
doi:10.1371/journal.pcbi.1000328.g002

firing rate $r(t)$ (Eq. 19). We here assume exponentially decaying temporal coupling kernels (Eq. 20) which allows for a mapping of the integral equation to a set of differential equations [5,14].

The four terms within the large parentheses on the right hand side of Eq. (1) can be interpreted as four contributions to the input current entering the somas of neurons in the layer-4 population. The first and second terms correspond to *feedforward* excitation $\left(\beta_{\mathrm{Ef}}\left[h_{\mathrm{Ef}}*r_{\mathrm{T}}^{\mathrm{x}}\right](t)\right)$ and inhibition $\left(\beta_{\mathrm{If}}\left[h_{\mathrm{If}}*r_{\mathrm{T}}^{\mathrm{x}}\right](t)\right)$ from the thalamus, respectively. The coupling kernel $h_{\mathrm{Ef}}(t)$ can be interpreted as the weight of the excitatory contribution to the present current input to the layer-4 population due to firing that has occurred in the thalamic population a time t in the past. Likewise, the third and fourth terms correspond to *recurrent* excitation $(\beta_{\mathrm{Er}}[h_{\mathrm{Er}}*r_4](t))$ and inhibition $(\beta_{\mathrm{Ir}}[h_{\mathrm{Ir}}*r_4](t))$ from cortical layer-4 neurons. The model structure is illustrated in Fig. 3B. Note that corticothalamic feedback [25] is not explicitly modeled as this effect will only change the thalamic firing rate. Since we do not model the thalamic firing rates and instead use the experimentally extracted $r_{\mathrm{T}}^{\mathrm{x}}$ as input to the model, any effect of cortical feedback affecting the thalamic firing rate will be included automatically.

The function $F_4(\cdot)$ in Eq. (1) is an *activation function* that converts the net input current to population firing rate $r_4(t)$. This activation function is often modeled as a sigmoidal function [4,8], but here we found that a simpler four-parameter threshold-type function

with a linear and/or parabolic activation above threshold provided a better fit to the experimental data, cf. Eq. (21). The form of this activation function is illustrated in Fig. 3A. Such a threshold-type activation function has also been seen experimentally when studying firing characteristics of excitatory neurons in the barrel column [26].

The temporal coupling kernel $h(t)$ is described by two parameters, a time constant τ and a time-delay parameter Δ, cf. Eq. (20). To reduce the number of parameters in the model in Eq. (1), the time delays in the recurrent temporal kernels are set to zero, i.e., $\Delta_{\mathrm{Er}} = \Delta_{\mathrm{Ir}} = 0$. Further, one of the weight parameters β can be fixed without loss of generality. We therefore set $\beta_{\mathrm{Ef}} \equiv 1$. Nevertheless, this full thalamocortical model encompasses 13 parameters (4 for the activation function, 3 weights, 6 specifying temporal kernels). This is a sizable number of adjustable model parameters given the variability of the experimental data, and when comparing with our experimental data it was observed that in particular the feedforward and recurrent inhibition terms had strongly overlapping effects on the model predictions for the layer-4 firing rate so that their individual contributions were difficult to assess. We thus chose to mainly investigate reduced versions of the full thalamocortical model in Eq. (1) where either (1) only the recurrent inhibition term ('recurrent' model) or (2) only the feedforward inhibition term ('feedforward' model) was kept, respectively.

A
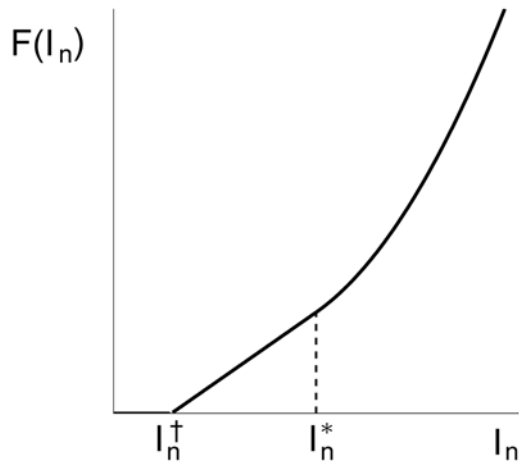
$$r_4(t) = F_4(I_4(t)), \; I_4(t) \equiv \left[h_{\mathrm{Ef}} * r_{\mathrm{T}}^{\mathrm{x}} \right](t) +$$
$$\left[(\beta_{\mathrm{Er}} h_{\mathrm{Er}} - \beta_{\mathrm{Ir}} h_{\mathrm{Ir}}) * r_4 \right](t) \tag{2}$$

This model has a special significance in that it maps (by use of the linear chain trick [14]) to a set of differential equations that are structurally similar to the firing-rate model suggested by Pinto et al. [8,9], cf. Eqs. (28–29) in Materials and Methods.

The model was fitted to the experimentally extracted population firing rate $r_4^x(t)$ (for all 27 stimulus conditions simultaneously) by minimizing the mean square deviation between model and experimental results (Eq. 22) using the optimization method described in Materials and Methods.

Fits to recurrent model. As illustrated in Fig. 4 the recurrent model successfully accounts for the experimental observations in all six experiments considered. In the panels each dot corresponds to an experimentally measured layer-4 firing rate $r_4^x(t_i)$ at a particular time t_i plotted against the value I_4 predicted by the fitted model at the same time t_i. If the model was perfect and the data noiseless, these points should all lie on the solid line corresponding to the fitted value of the activation function $F_4(I_4)$. A small spread is generally observed in Fig. 4, and this is reflected by the low error value, i.e., ε in Eq. (22), of the best fits. As seen is Table 1 the errors are all less than 6%. In Table 1 we also list the fitted parameter values for the six experiments.

Fitted model parameters for recurrent model. Experiments 1–3 correspond to the stimulus paradigm with 3 different amplitudes and 9 different rise times, while experiments 4–6 correspond to 27 different amplitudes but a single fixed rise time. As seen, for example, in Fig. 2 the variation in the rise time affects the thalamic and cortical responses more than variation in the stimulus amplitude. Thus experiments 1–3 exhibit a greater variation in the responses and thus a richer data set for the models to be tested against. In fact, for experiments 4–6 only a parabolic part of the activation function $F_4(I_4)$ could be seen in the data, and the linear part of the activation function in Eq. (21) was omitted from the model.

The choice of stimuli set also appears to affect the fitted parameter values somewhat as indicated by comparing the fitted parameter values for experiments 1, 2, 4 and 5, all carried out using the same preparation in the same rat. As seen in Table 1 the fitted parameter values of experiment 1 and 2 are very similar, likewise for experiment 4 and 5. The parameter values for experiments 1 and 2 also compare well with the values for experiments 4 and 5, but less so. In the following we will focus mostly on experiments 1–3 where the 3×9 stimulus paradigm is used, and a more varied set of responses are obtained.

For experiments 1 and 2 the fitted feedforward time constants τ_{Ef} are between 3 and 6 milliseconds and the feedforward delay Δ_{Ef} between 2 and 3 milliseconds (see Table 1). The recurrent time constants are significantly longer: between 8 and 10 milliseconds for the recurrent excitation τ_{Er} and between 13 and 15 milliseconds for the recurrent inhibition τ_{Ir}. For all six experiments we observe the recurrent inhibition to have the longest time constant. In experiments 3 and 6 the fitted time constant of the feedforward excitation is seen to be longer than for the recurrent excitation.

In all experiments the weight of the recurrent inhibition β_{Ir} was found to be larger than the weight of the recurrent excitation β_{Er}. However, the values of β_{Er} and β_{Ir} are seen to vary significantly between the experiments. This partially reflects that when the recurrent terms dominate the feedforward term, large values of the

B
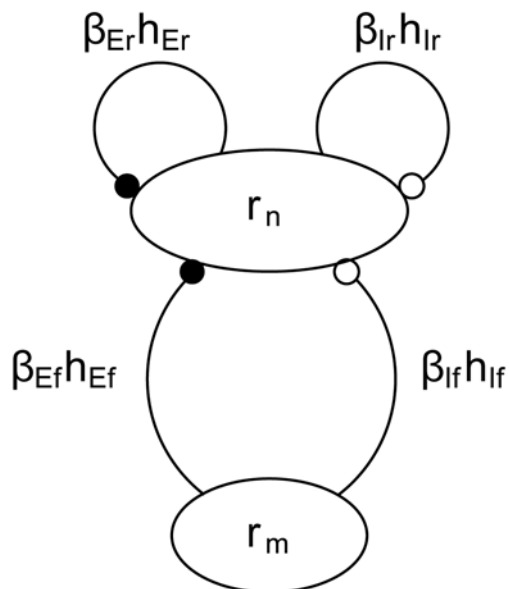
Figure 3. Model structure. (A) Illustration of form of activation function $F_n(I_n)$ in Eq. (21). (B) Illustration of structure of population firing-rate models with feedforward and recurrent terms in Eqs. (1) and (10). Filled and open dots represent excitatory and inhibitory connections, respectively.
doi:10.1371/journal.pcbi.1000328.g003

Recurrent thalamocortical model

We first consider the so called *recurrent* thalamocortical model where the feedforward inhibitory term in the full model in Eq. (1) has been omitted, i.e.,

Figure 4. Fits of recurrent thalamocortical model. Illustration of fits of recurrent thalamocortical model in Eq. (2) to data from experiments 1–6. Each black dot corresponds to the experimentally measured layer-4 firing rate $r_4^x(t_i)$ at a specific time point t_i plotted against the model value of $I_4(t_i)$. The red dots are corresponding experimental data points taken from the first 5 ms after stimulus onset (for all 27 stimuli). Thes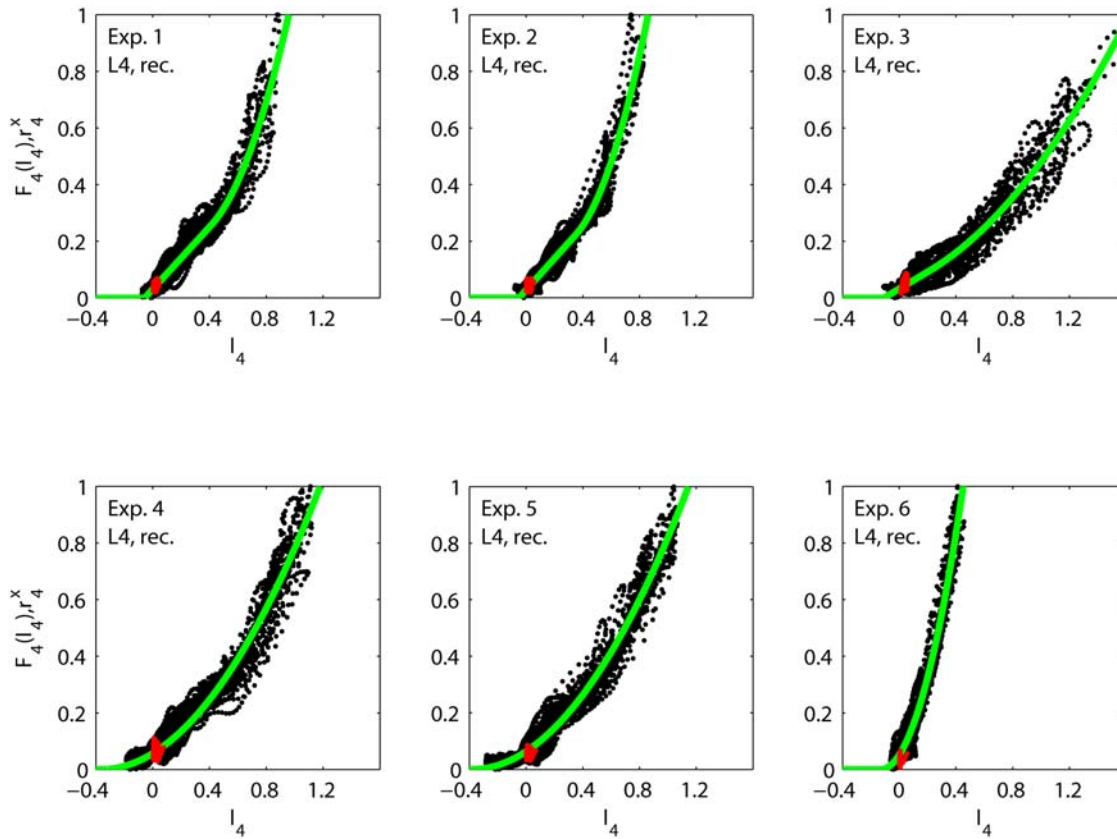e data points show the activity prior to any stimulus-evoked thalamic or cortical firing and correspond to background activity. The solid green curve corresponds to the fitted model activation function $F_4(I_4)$.
doi:10.1371/journal.pcbi.1000328.g004

recurrent weights can be compensated by making the activation function less steep, and vice versa. However, the ratio β_{Er}/β_{Ir} is found to be rather constant, typically between 0.75 and 0.9 (with experiment 6 as the only exception). Thus while excitation may dominate at short time scales due to the shorter excitatory time constants, inhibition dominates at longer time scales.

The positive correlation between β_{Er} and β_{Ir} was confirmed by direct inspection of the correlation matrices for the ensembles of fitted model parameters obtained during the numerical optimization procedure (Materials and Methods). It was also seen by inspection of the eigenvectors of the most 'sloppy' direction of the Levenberg-Marquardt Hessian **L** (Eq. 23), i.e., the component with the smallest eigenvalue. A 'sloppy' direction of **L** means that the fitting error ε will change little when moving along this direction in parameter space [27]. A positive correlation between β_{Er} and β_{Ir} would imply that the fitting error will change little when both parameters are increased (or decreased) simultaneously. Indeed, the eigenvector of the most 'sloppy' eigenvalue revealed exactly this property.

Further inspection revealed that β_{Er} is negatively correlated with the slope of the activation function (parameters a and b in Eq. (21)). This is as expected since a decrease in the recurrent excitatory weight β_{Er} can be compensated for by an increase in the activation-function slope. Moreover, it was observed that β_{Er} (and β_{Ir}) is positively correlated to τ_{Er} and negatively correlated to τ_{Ir}.

Phase-plane analysis of recurrent model. The identified recurrent thalamocortical models on integral form can be mapped to a corresponding set of two differential firing-rate equations using the 'linear-chain trick' [5,14] as described in Materials and Methods, cf. Eqs. (25–29). This is very useful since it allows for the use of standard techniques from dynamical systems analysis to investigate the identified models.

With slightly redefined auxiliary variables compared to Eqs. (25–27) in Materials and Methods, that is,

$$X_{E4} \equiv [h_{Er} * r_4](t), \; X_{I4} \equiv [h_{Ir} * r_4](t), \; X_T(t) \equiv [h_{Ef} * r_T](t), \quad (3)$$

the recurrent thalamocortical model can be reformulated as (cf. Eqs. 28–29)

$$\tau_{Er}\frac{dX_{E4}}{dt} = -X_{E4} + F_4(\beta_{Er}X_{E4} - \beta_{Ir}X_{I4} + \beta_{Ef}X_T(t)), \quad (4)$$

$$\tau_{Ir}\frac{dX_{I4}}{dt} = -X_{I4} + F_4(\beta_{Er}X_{E4} - \beta_{Ir}X_{I4} + \beta_{Ef}X_T(t)) \quad (5)$$

This equation set resembles the model derived using 'semirigorous' techniques by Pinto et al. in [8], and further explored in [9], for populations of interconnected layer-4 excitatory and inhibitory barrel neurons receiving stimulus-evoked thalamic input.

The formulation in terms of two dynamical variables X_{E4} and X_{I4}, with X_T only providing an external input, allows for

Table 1. Fitted model parameters for recurrent thalamocortical model.

	Exp. 1	Exp. 2	Exp. 3
τ_{Ef} (ms)	3.7	5.7	3.3
Δ_{Ef} (ms)	2.5	2.0	4.5
τ_{Er} (ms)	9.3	8.0	1.3
τ_{Ir} (ms)	13.7	14.8	30.6 ± 0.7
β_{Er}	4.27 ± 0.03	2.93 ± 0.16	1.26 ± 0.03
β_{Ir}	4.81 ± 0.03	3.85 ± 0.16	1.48 ± 0.02
β_{Er}/β_{Ir}	0.89	0.76 ± 0.01	0.85 ± 0.02
a_4	0.55	0.56	0.30
b_4	1.48	1.88 ± 0.01	0.26 ± 0.02
$I_4^{\dagger}$	-0.06	-0.05	-0.11
I_4^{*}	0.41	0.35	0.21
error (ε)	0.0522	0.0430	0.0586
	Exp. 4	Exp. 5	Exp. 6
τ_{Ef} (ms)	2.8	1.9	8.2
Δ_{Ef} (ms)	3.5	4.0	3.5
τ_{Er} (ms)	14.7	15.7	3.3
τ_{Ir} (ms)	20.3	22.9	19.6
β_{Er}	5.98 ± 0.07	6.15 ± 0.01	0.61
β_{Ir}	6.65 ± 0.07	7.53 ± 0.01	2.06
β_{Er}/β_{Ir}	0.90	0.82	0.29
a_4	-	-	-
b_4	0.42	0.43	2.94
$I_4^{\dagger}$	I_4^{*}	I_4^{*}	I_4^{*}
I_4^{*}	-0.37	-0.39	-0.13
error (ε)	0.0414	0.0371	0.0397

Resulting optimized parameters for the recurrent thalamocortical network model (Eq. 2) incorporating feedforward excitation and recurrent excitation and inhibition. The listed parameter values correspond to the mean of fitted parameter values from 25 selected models giving essentially the same error (see Materials and Methods). The standard deviations are only listed if they exceed the last digit of the mean. Note that the value of β_{Er}/β_{Ir} is included to illustrate the relative constancy of the ratio of the fitted values for β_{Er} and β_{Ir}.
doi:10.1371/journal.pcbi.1000328.t001

visualization of the circuit behavior using phase-plane analysis. In analogy with Pinto et al. [9] we show in Fig. 5 the layer-4 model response for the weakest ($a1,t9$) and strongest ($a3,t1$) stimuli for experiment 1. In the five phase plots for the two stimuli considered the *instantaneous* excitatory and inhibitory nullclines at five different times ($t_{wi}, i = 1, \ldots, 5$, for weak stimulus; $t_{si}, i = 1, \ldots, 5$, for strong stimulus) are shown. These nullclines are obtained assuming a constant thalamic synaptic drive equal to the instantaneous values $X_T(t_{wi})$ or $X_T(t_{si})$. Below the instantaneous excitatory (inhibitory) nullcline dX_{E4}/dt (dX_{I4}/dt) is negative, and the color code illustrates the magnitude of dX_{E4}/dt.

As seen in Fig. 5 the network model for the strong stimulus ($a3,t1$) makes a significantly more extended excursion in the (X_{E4}, X_{I4}) phase plane than the weaker stimulus ($a1,t9$). This can be readily understood by investigation of the phase-plane plots for the times shortly after onset. For the strong stimulus the trajectory is seen to be in a region with a large dX_{E4}/dt at, for example, the times t_{s1} and t_{s2} resulting in a rapid growth and large maximum

value of X_{E4}. For these short times the fast feedforward and recurrent excitation dominates the slower inhibition. For the weak stimulus, however, the trajectory remains in regions with small values of dX_{E4}/dt (i.e., without dominant excitation). As a consequence we observe that while the difference in maximum amplitude of the thalamic synaptic drives between the strong and weak stimuli is seen in the upper panels of Fig. 5 to be less than a factor two, the difference in the maximum layer-4 firing rate is more than a factor three. Thus the amplitude of the thalamic population response does not explain the layer-4 response alone; the rise time of the thalamic response is also important [9].

The qualitative conclusions from Fig. 5 is in agreement with the corresponding analysis by Pinto et al. [9]. This is an interesting result in itself since our model and the model of Pinto et al. [9] are derived in very different ways. Here the parameters are extracted from a single experiment measuring population activity directly. By contrast, in the study by Pinto et al. the model and its parameters were chosen to qualitatively reproduce pooled barrel population responses, i.e., single-unit poststimulus time histograms (PSTHs), recorded from numerous animals [8,9]. Further, the thalamic responses used to generate their phase-plots analogous to Fig. 5 were modeled with a simplified triangular temporal rate profile with varying rise times [9], not extracted from experimental data like here.

Due to differences between our model (Eqs. 4–5) and the model of Pinto et al. [9] a direct comparison between the applied model parameters is generally not possible. However, the time constants can be compared directly: their choice of $\tau_{Er} = 5$ ms and $\tau_{Ir} = 15$ ms is qualitatively similar to what was extracted from our experiments 1 and 2, i.e., $\tau_{Er} = 8$–10 ms and $\tau_{Ir} = 13$–15 ms. Their choice of weight parameters appears to differ more from our results: for example, they set the ratio β_{Er}/β_{Ir} to be between 1.7 and 2.3, i.e., stronger recurrent excitation than recurrent inhibition. For experiments 1–3 we see in Table 1 that the ratio is found to be between 0.75 and 0.9, i.e., the recurrent inhibition has a larger weight than recurrent excitation. For the *tension*, i.e., the ratio of recurrent excitation over the excitation from thalamus β_{Er}/β_{Ef} [8], they chose a value of about 0.9. For our experiments this ratio showed a significant variation, varying from 1.3 to 4.3 for experiments 1–3.

Stability of background states for recurrent model. On differential form our population-firing rate model is readily available for stability analysis. Due to the recurrent excitatory term the recurrent thalamocortical model can in principle have unstable equilibrium points, but the identified models must clearly exhibit stable background states when only the stationary thalamic input (corresponding to the absence of whisking) is present. For experiments 1–3 the background state (cf. red dots in Fig. 4) is found to be on the linear flank of the activation function, and the stability of these background states can be demonstrated on the basis of the fitted model parameters $a_4, \tau_{Er}, \tau_{Ir}, \beta_{Er}, \beta_{Ir}$ listed in Table 1. A full stability analysis for the recurrent thalamocortical model is given in Materials and Methods (Eqs. 30–35), and the criteria for stability of the background state is found to be

$$1 + \frac{\tau_{Er}}{\tau_{Ir}} + a_4 \left(\beta_{Ir} \frac{\tau_{Er}}{\tau_{Ir}} - \beta_{Er} \right) > 0 \qquad (6)$$

$$1 + a_4 (\beta_{Ir} - \beta_{Er}) > 0 \qquad (7)$$

Insertion of the fitted numerical parameter values into the inequalities Eqs. (6–7) demonstrates that both conditions are
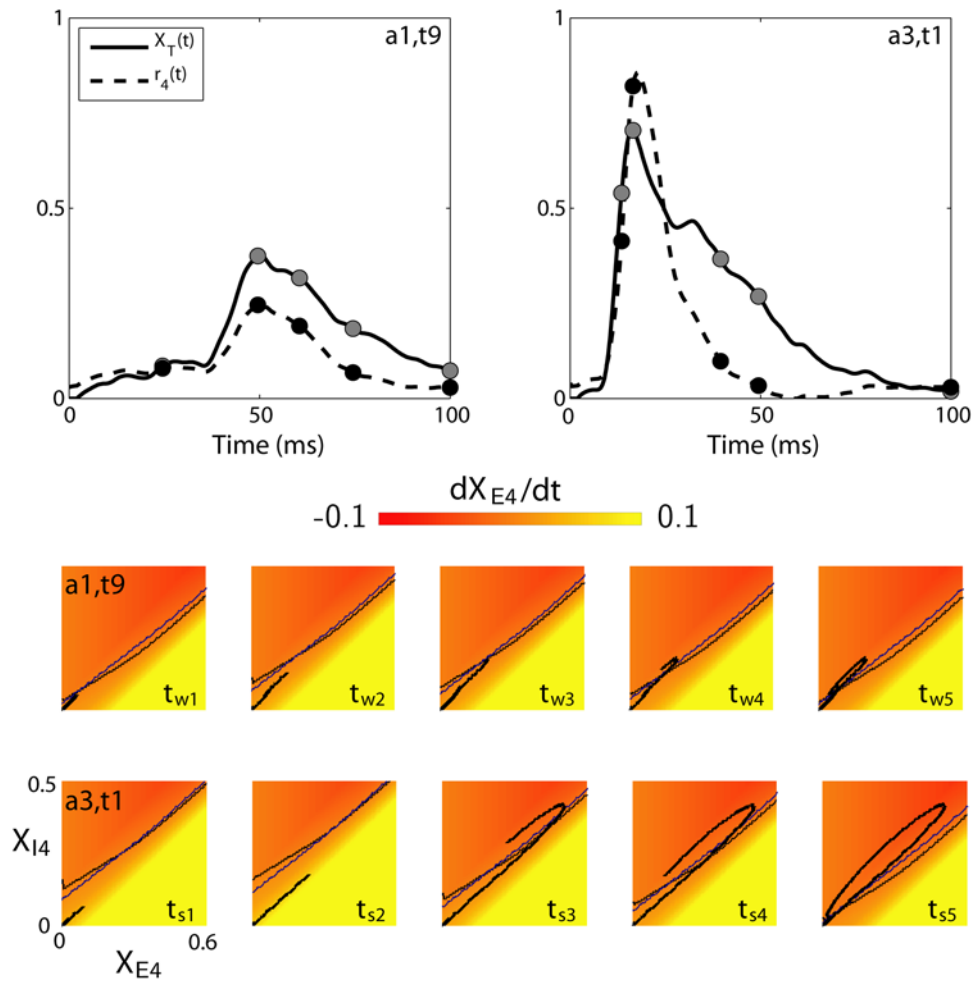
Figure 5. Phase-plane analysis of recurrent thalamocortical model for experiment 1. Phase-plane analysis of recurrent thalamocortical model in Eqs. (4–5) for fitted model parameters for experiment 1, cf. Table 1. Upper panels show the synaptic drive from thalamus $X_\mathrm{T}(t)$ and the firing rate $r_4(t) = F_4(\beta_\mathrm{Er} X_\mathrm{E4}(t) - \beta_\mathrm{Ir} X_\mathrm{I4}(t) + X_\mathrm{T}(t))$ for the weakest ($a1,t9$; left) and strongest ($a3,t1$; right) stimuli. The filled dots in the two upper panels show the points in time, $t_{\mathrm{w}i}(i=1,\ldots,5)$ for $(a1,t9)$ and $t_{\mathrm{s}i}(i=1,\ldots,5)$ for $(a3,t1)$ at which the network states are shown in the two lower panels. In each of the phase plots (five for each of the stimuli) the *instantaneous* excitatory (black) and inhibitory (blue) nullclines are shown, i.e., the nullclines obtained with a constant thalamic synaptic drive equal to the instantaneous value $X_\mathrm{T}(t_{\mathrm{w}i})$ for $(a1,t9)$ and $X_\mathrm{T}(t_{\mathrm{s}i})$ for $(a3,t1)$. The network's activity is indicated by the black response curve, where the head of the curve marks the network's current state, and the tail represents prior states.
doi:10.1371/journal.pcbi.1000328.g005

fulfilled and that the background state is indeed stable. Inspection of Eqs. (6–7) further shows that instability is promoted by an increased weight of the recurrent excitation (β_Er), an increased slope of the activation function (a_4), or an increased time constant of the recurrent inhibition (τ_Ir) [28]. For example, for experiment 1 the background state becomes unstable if β_Er is increased by a factor 1.5, a_4 by a factor 3.2, or τ_Ir by a factor 1.9.

Inclusion of feedforward inhibition in thalamocortical model fits

We further investigated whether the full thalamocortical model in Eq. (1), i.e., the recurrent model amended with the feedforward inhibition term $\left(\beta_\mathrm{If} h_\mathrm{If} * r_\mathrm{T}^\mathrm{x}\right)$, gives an improved fit compared to the recurrent model (Eq. 2) alone. Numerical investigations showed that the improvement, i.e., reduction of the error ε, was marginal: for experiments 1–3 the reduction in error was in all cases less than 0.001. Thus the recurrent inhibitory term alone seems to be sufficient to account well for the present experimental data.

We then investigated whether a pure *feedforward* model, i.e., a model with feedforward excitation and inhibition only, could account for the thalamocortical data. This model reads

$$r_4(t) = F_4\left(\left[(\beta_\mathrm{Ef} h_\mathrm{Ef} - \beta_\mathrm{If} h_\mathrm{If}) * r_\mathrm{T}^\mathrm{x}\right](t)\right) \tag{8}$$

and in Table 2 and Fig. 6 we show the results of the optimization.

Comparison of fits to recurrent and feedforward thalamocortical models

For experiments 1–3, which exhibit the largest variation of responses, the fits of the experimental data for the feedforward model are poorer than for the corresponding fits of the recurrent model. While the errors ε for the recurrent model are seen in Table 1 to be 0.052, 0.043 and 0.059 for experiments 1, 2 and 3, respectively, the corresponding errors for the purely feedforward model are seen in Table 2 to be 0.064, 0.069 and 0.071, i.e., relative increases in errors of 23%, 60% and 20%, respectively. However, for experiments 4–6 where only the stimulus amplitude

Table 2. Fitted model parameters for feedforward thalamocortical model.

	Exp. 1	Exp. 2	Exp. 3
τ_{Ef} (ms)	8.4	9.8	9.3
Δ_{Ef} (ms)	2.5	3.5	5.0
τ_{If} (ms)	20.5±0.3	18.2±0.1	100[*]
Δ_{If} (ms)	2.5	3.5	5.0
β_{If}	0.94	1.06	3.61
a_4	0.28±0.02	0.54±0.01	0.14
b_4	8.9±0.2	29.5±1.2	16.2±0.3
$I_4^{\dagger}$	−0.15±0.01	−0.11	−0.52
I_4^{*}	−0.03	−0.00	0.02
error (ε)	0.0636	0.0691	0.0706
	Exp. 4	**Exp. 5**	**Exp. 6**
τ_{Ef} (ms)	8.5	5.2	5.1
Δ_{Ef} (ms)	2.5	3.0	5.0
τ_{If} (ms)	93.5±0.2	87.3±0.6	17.7±0.4
Δ_{If} (ms)	2.5	1.5	5.0
β_{If}	1.8	2.0	1.3
a_4	0.09	0.05	0.01
b_4	3.2	1.9	8.7±0.4
$I_4^{\dagger}$	−0.54	−0.76±0.02	−5.80±1.1
I_4^{*}	−0.06	−0.13	−0.07
error (ε)	0.0394	0.0351	0.0629

Resulting optimized parameters for the feedforward thalamocortical network model (Eq. 8) incorporating feedforward excitation and inhibition. The listed parameter values correspond to the mean of fitted parameter values from 25 selected models giving essentially the same error (see Materials and Methods). The standard deviations are only listed if they exceed the last digit of the mean. Note that for experiments 4–6 the parameter a_4 was fixed to zero in the optimization procedure. Also, for experiment 3 the listed value 100 ms for τ_{If} corresponds to the maximum allowed value for this parameter.
doi:10.1371/journal.pcbi.1000328.t002

and not the rise time is varied, there is no such clear preference, i.e., lower fitting errors, for the recurrent model.

In Fig. 7 we compare the best fits of the recurrent (Eq. 2) and feedforward (Eq. 8) thalamocortical models with the experimentally extracted layer-4 firing rate for experiment 1 for the 9 stimulus conditions depicted in Fig. 2. Both models underestimate the peak values for the layer-4 firing rate for the shortest rise time ($t1$) giving the largest responses. For the stimulus $a3,t1$ giving the overall largest layer-4 response, the fitted recurrent model both follows the rise and the ensuing fall of the response peak better than the feedforward model, but this difference is less pronounced for the other stimuli providing the larger responses. A detailed investigation of the fits for individual stimulus conditions in fact shows that the fitted recurrent model typically is closer to the experimental curves than the feedforward model for the entire set of stimulus conditions (data not shown).

The fitted activation functions for the recurrent and feedforward models for experiments 1 to 3 are quite different (cf. Figs. 4 and 6). In particular, for experiments 1 and 2 the activation functions for recurrent models have pronounced linear flanks which cover about half the dynamic range of I_4. In contrast, the activation functions of the feedforward models for these two experiments are essentially parabolic in the entire dynamic range. In the recurrent model the 'boosting' of the salient stimuli thus appears to a large extent to be provided by recurrent excitation allowing for a partially linear activation function. In contrast, in the feedforward model the observed amplification of strong stimuli requires a purely parabolic activation function.

Another way to compare the candidate thalamocortical models is to investigate their so called 'sloppiness' [27]. Sloppiness is a measure of the sensitivity of the model fit to changes in model parameters: large sloppiness means that some parameter combinations can be varied significantly without changing the quality of the model fit. Sloppiness can be quantified by an eigenvalue analysis of the Hessian matrix composed of the partial 2nd derivatives of the model error function [27,29]. Here the so called Levenberg-Marquardt Hessian matrix $\mathbf{L}$ (Eq. 23) is used, cf. Materials and Methods. Fig. 8 shows the eigenvalue spectra of $\mathbf{L}$ (23) for experiments 1–3 for the three investigated thalamocortical models: (1) the recurrent model (Eq. 2), (2) the feedforward model (Eq. 8), and (3) the full model including both feedforward inhibition and the recurrent connections (Eq. 1). The spectra are
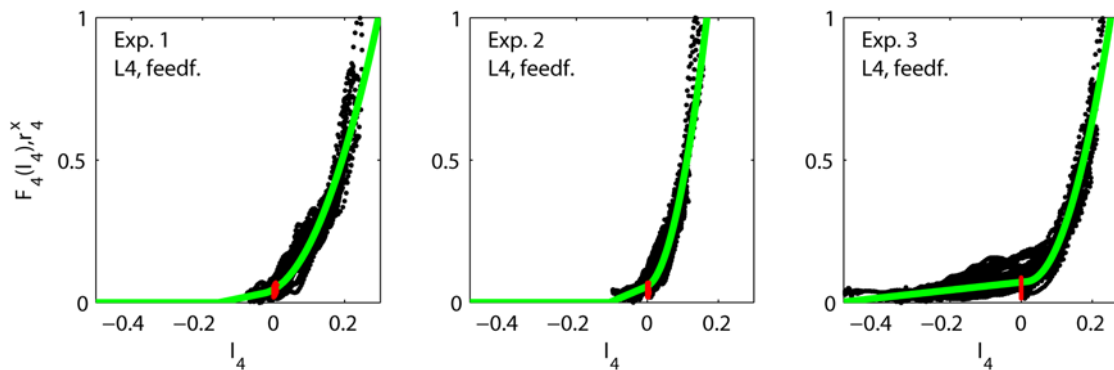

Figure 6. Fits of feedforward thalamocortical model. Illustration of fits of feedforward thalamocortical model (Eq. 8) to data from experiments 1–3. Each dot corresponds to the experimentally measured layer-4 firing rate $r_4^x(t_i)$ at a specific time point t_i plotted against the model value of $I_4(t_i)$. The red dots are corresponding experimental data points taken from the first 5 ms after stimulus onset (for all 27 stimuli). These data points show the activity prior to any stimulus-evoked thalamic or cortical firing and represent background activity. The solid green curve corresponds to the fitted model activation function $F_4(I_4)$.
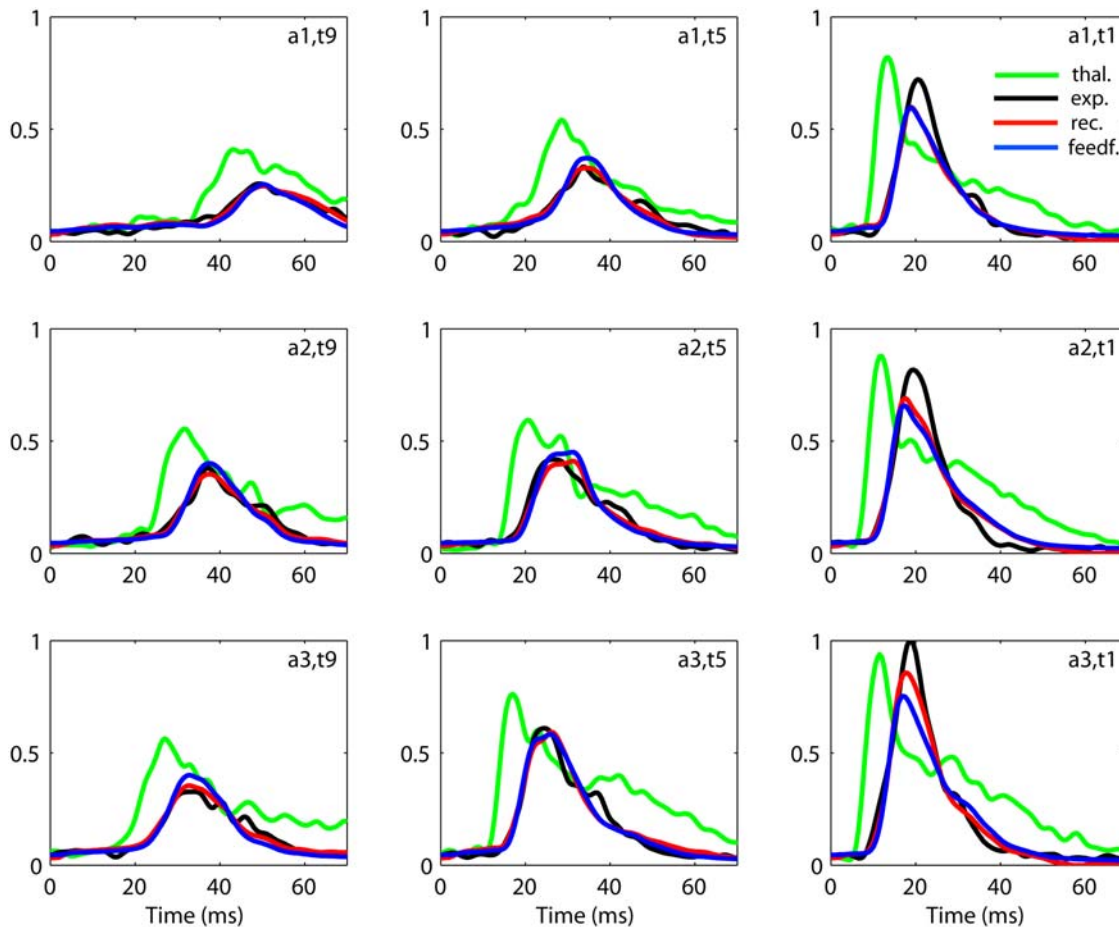doi:10.1371/journal.pcbi.1000328.g006

Figure 7. Comparison of thalamocortical model fits. Comparison of fits of the recurrent and feedforward thalamocortical models with experimental data set 1 for the same 9 (of 27) stimulus conditions considered in Fig. 2. The green line corresponds to the thalamic input firing rate $r_T^x(t)$, the black line to the experimentally extracted layer-4 firing rate $r_4^x(t)$, while the red and blue lines correspond to the best fits of the recurrent (Eq. 2) and feedforward (Eq. 8) models for the layer-4 firing rate $r_4(t)$, respectively. Time zero corresponds to stimulus onset.
doi:10.1371/journal.pcbi.1000328.g007

normalized so that the largest eigenvalue is unity. Small eigenvalues correspond to large sloppiness, and variations in model parameters along the direction of the corresponding eigenvectors in parameter space will have small effects on the overall model error [27]. The number of eigenvalues corresponds to the dimension of **L**. The feedforward delay parameters Δ_{mn}, which are discrete parameters in the present modeling scheme, are absent in **L** (cf. Materials and Methods), and the number of eigenvalues in Fig. 8 is thus nine for the recurrent model, seven for the feedforward model, and eleven for the full model.

In Fig. 8 we see more 'sloppy' eigenvalues for the feedforward model than the recurrent model. For example, only one of nine eigenvalues is found to be less than $2 \cdot 10^{-5}$ (measured relative to the largest eigenvalues) for the recurrent model. In contrast, two of seven eigenvalues are less than $2 \cdot 10^{-5}$ for the feedforward model. This larger 'sloppiness' is in accordance with the poorer fits observed for the feedforward model; the functional flexibility inherent in the feedforward model appears not to be well suited to account for the present data with 3 different amplitudes and 9 different stimulus rise times. For the full model we find three of eleven eigenvalues to be smaller than 10^{-5}. Thus compared to the recurrent model, the added feedforward inhibition with two new parameters seems only to add two 'sloppy' eigenvalues, in line with the observation that the overall fit is not improved much.

To summarize, our results so far suggest that the model with recurrent inhibition accounts slightly better for the present experimental data than the model with feedforward inhibition, i.e., that the layer-4 interneurons providing the inhibition of the layer-4 excitatory neurons are in turn mainly driven by excitation from layer-4 neurons. Since the relative strength of recurrent effects compared to feedforward effects appears to increase with increasing thalamic stimuli [19], this might indicate that the present fits to the experimental data might be dominated by 'strong' inputs. To explore this further we investigated the properties of the thalamocortical transfer using linear-systems measures such as transfer functions in frequency space and impulse-response functions.

Thalamocortical transfer

Thalamocortical frequency response. Our identified thalamocortical models are in general nonlinear due to the nonlinear activation functions $F_4(I_4)$. For small deviations around a working point, however, the above models can be linearized, so that linear-systems measures such as *transfer functions* in frequency space and *impulse-response functions* can be explored [30].

For the thalamocortical models the derivation of the transfer function amounts to deriving the response to a small sinusoidal modulation $\tilde{r}_T(\omega)$ in the thalamic input superimposed on a constant background activity r_{T0}. As shown in Materials and
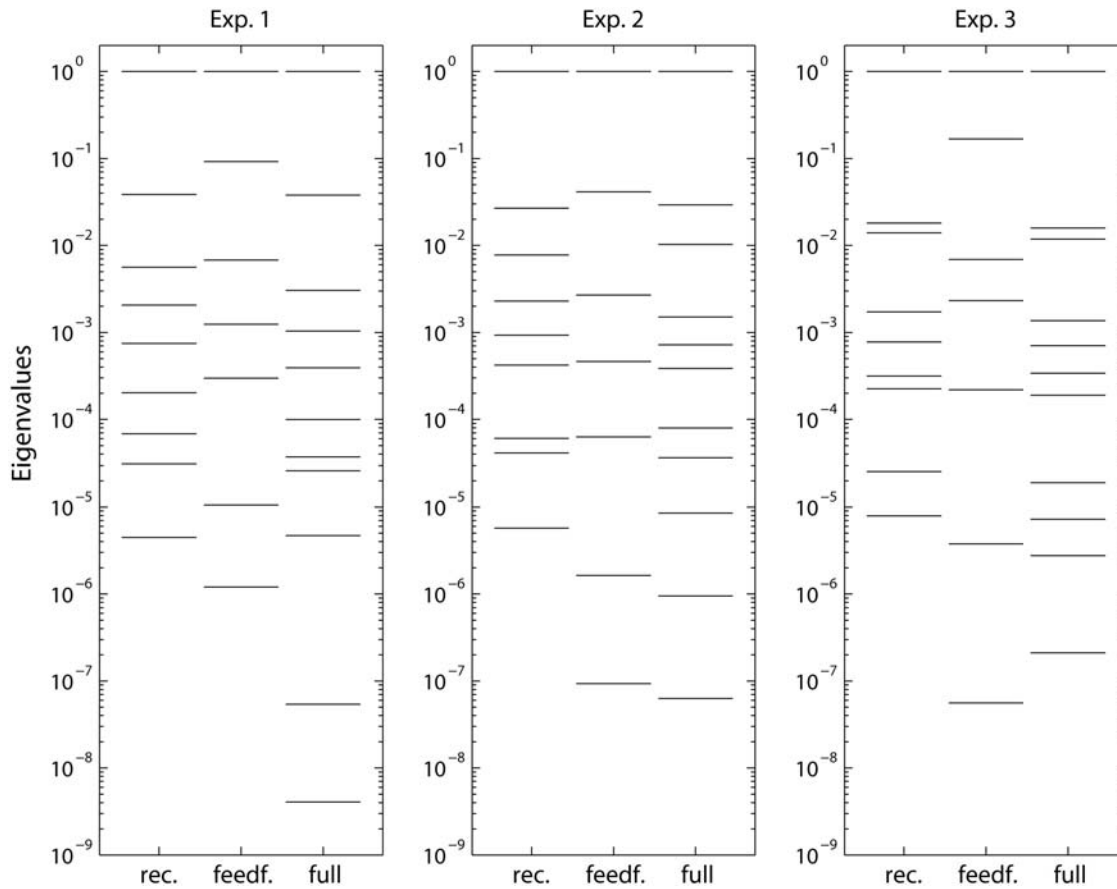
Figure 8. Sloppiness analysis of thalamocortical model. Illustration of parameter sensitivities, i.e., 'sloppiness', of model fits for recurrent (*rec.*), feedforward (*feedf.*) and full (*full*) thalamocortical models corresponding to Eqs. (2), (8), and (1), respectively. Eigenvalue spectra of the Levenberg-Marquardt Hessian **L** (Eq. 23) for experiments 1–3 are shown. The eigenvalues are normalized to the largest eigenvalue. Delay parameters Δ_{mn} are left out of the analysis, since in our models these parameters are set to be discrete (with a time step of 0.5 ms).
doi:10.1371/journal.pcbi.1000328.g008

Methods the modulated response $\tilde{r}_4(\omega)$ (complex notation) in layer 4 is then given by $\tilde{r}_4(\omega) = T_{4/T}(\omega)\tilde{r}_T(\omega)$ where $T_{4/T}(\omega)$ is the linear *transfer function* [30–32]. The transfer function for the full thalamocortical model Eq. (1) is derived in Materials and Methods, cf. Eq. (42), and for the *recurrent* model in Eq. (2) it reduces to

$$T_{4/T}(\omega) = \frac{\tilde{r}_4(\omega)}{\tilde{r}_T(\omega)} = \frac{F_4'(I_{40})\tilde{h}_{Ef}(\omega)}{1 - F_4'(I_{40})\beta_{Er}\tilde{h}_{Er}(\omega) + F_4'(I_{40})\beta_{Ir}\tilde{h}_{Ir}(\omega)} \quad (9)$$

Here β_{Ef} and β_{If} in Eq. (42) has been set to one and zero, respectively. $F_4'(I_{40})$ is the derivative of the activation function at the working point I_{40}, and the Fourier-transformed coupling kernels $\tilde{h}_{Ef}(\omega), \tilde{h}_{If}(\omega), \tilde{h}_{Er}(\omega), \tilde{h}_{Ir}(\omega)$ are all given by $\tilde{h}(\omega) = exp(i\omega\Delta)/(1 - i\tau\omega)$, cf. Eq. (39).

This transfer function describes how a small modulation of the thalamic population firing rate transfers to the layer-4 population firing rate. The transfer function $T_{4/T}(\omega)$ is a complex quantity where the transfer amplitude is given by the absolute value $|T_{4/T}(\omega)|$, and the change in phase between the thalamic input and layer-4 output is given by the complex phase angle.

Fig. 9 shows an example of how the Fourier amplitude (lower left) and phase (lower right) of the recurrent thalamocortical transfer-function model in Eq. (9) depends on frequency. The parameter

values correspond to the fitted values of $\beta_{Er}, \beta_{Ir}, \tau_{Ef}, \tau_{Er}, \tau_{Ir}$ and Δ_{Ef} for experiment 1 taken from Table 1. Since the fitted activation function $F_4(I_4)$ is nonlinear, there is no unique derivative $F_4'(I_4)$ for the fitted model. In Fig. 9 we thus show results for two different values of the derivative: (i) $F_4'(I_4) = a_4 = 0.55$ corresponding to the derivative on the linear flank, and (ii) $F_4'(I_4 = 0.5) = 0.81$ corresponding a larger derivative more characteristic for the parabolic part of the activation function. In both cases the amplitude of the model transfer function has its maximum at finite frequencies, 16 Hz and 18 Hz, respectively. This peak stems from a resonance-like phenomenon for frequencies where the denominator of Eq. (9) becomes small. Even larger values of $F_4'(I_4)$ would increase the peak value further.

In Fig. 9 (lower right) we further observe that the *phase* of the transfer function is negative for the smallest frequencies. The negative transfer-function phase implies that the maximum in the layer-4 responses will precede the maximum of the thalamic input for a small sinusoidal input for these frequencies.

Fig. 9 further shows the amplitude of the Fourier components of the thalamic input $r_T^x(\omega)$ (upper left), the layer-4 firing rate $r_4^x(\omega)$ (upper right), as well as the amplitude (lower left) and phase (lower right) of the experimental transfer ratio $r_4^x(\omega)/r_T^x(\omega)$ for six of the stimulus conditions providing the strongest response in experiment 1 (*a3,t1*; *a3,t2*; *a3,t3*; *a2,t1*; *a2,t2*; *a2,t3*). Also the average of the amplitudes and phases of the experimental transfer ratios across these six stimulus conditions are shown. The same
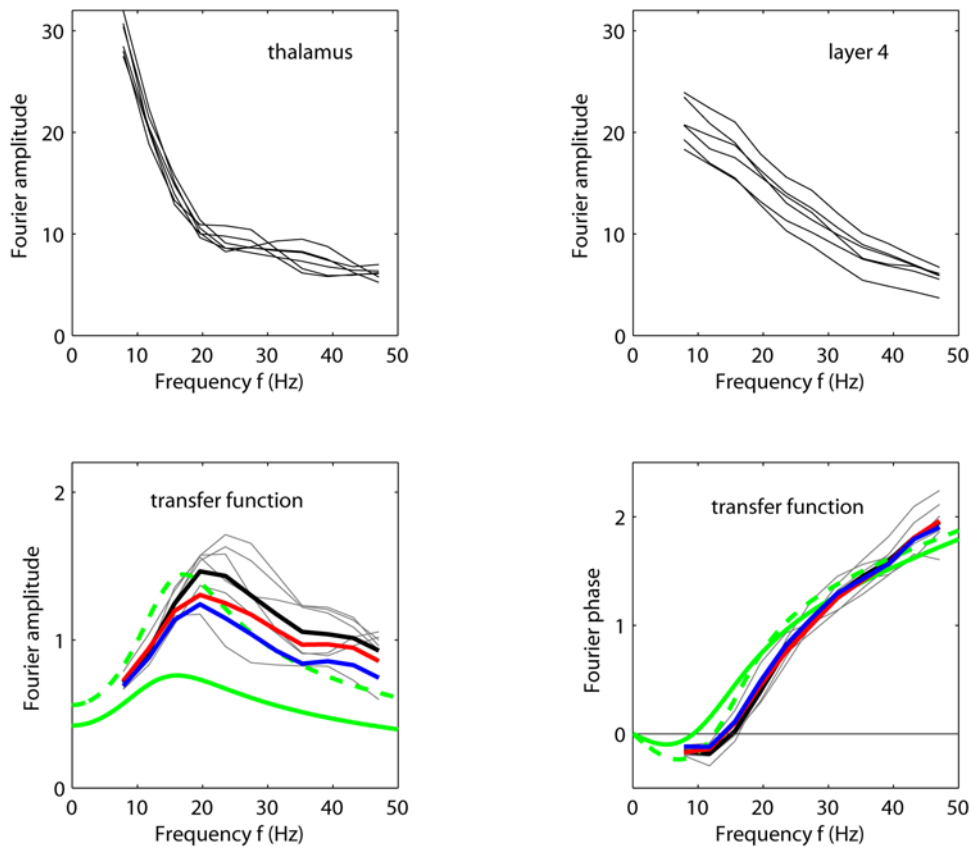
Figure 9. Thalamocortical transfer for experiment 1. Frequency content, i.e., Fourier amplitudes, of the thalamic input $r_T^x(2\pi f)$ (upper left) and the layer-4 firing rate $r_4^x(2\pi f)$ (upper right) for six stimulus conditions providing the strongest response in experiment 1 ($a3,t1$; $a3,t2$; $a3,t3$; $a2,t1$; $a2,t2$; $a2,t3$). (Note that $f = \omega/(2\pi)$.) The corresponding amplitude (lower left) and phase (lower right) of the experimental transfer ratio $r_4^x(2\pi f)/r_T^x(2\pi f)$ are shown as thin grey lines while the thick black lines represent the corresponding averages for these six stimuli. Examples of model predictions for amplitude (lower left) and phase (lower right) of the recurrent thalamocortical transfer-function model (Eq. 9) are shown for the fitted parameter values $\beta_{Er}, \beta_{Ir}, \tau_{Ef}, \tau_{Er}, \tau_{Ir}$ and Δ_{Ef} for experiment 1 taken from Table 1; green lines correspond to choosing $F_4'(I_4) = a_4 = 0.55$, and dashed green lines to $F_4'(I_4 = 0.5) = 0.81$. The red and blue lines in the lower panels correspond to the average of the amplitude (lower left) and phase (lower right) of the transfer ratios found for the six stimuli listed above when driving the fitted recurrent (red) and feedforward (blue) models in Eqs. (2) and (8), respectively, with the experimentally extracted thalamic input $r_T^x(t)$.
doi:10.1371/journal.pcbi.1000328.g009

characteristic resonance peak is seen in the experimental transfer ratios as for the linear-model transfer function in Eq. (9). The theoretical function for the largest shown value for $F_4'(I_4)$, i.e., $F_4'(I_4 = 0.5) = 0.81$, is seen to be closest to the experimental curves. This is not surprising since the depicted experimental curves correspond to six of the stimuli giving the largest responses for which also the parabolic part of the activation function is encountered. We see, however, that the maxima of the experimental transfer ratios are systematically shifted to somewhat higher frequencies compared to the predictions of the linear transfer-function model in Eq. (9). The same small deviation is also observed for the transfer ratio found by replacing $r_4^x(\omega)$ with the Fourier transform of the best fit $r_4(\omega)$ to the recurrent model in Eq. (2) (red curve in lower left panel of Fig. 9). Thus the deviation is presumably due to the non-linearities inherent in the system under the present stimulus condition, represented by the nonlinear activation function in the recurrent model. In Fig. 9 (lower right) we also observe a good qualitative agreement between the predicted phase difference between the thalamic input and layer-4 output from the linear transfer-function model and the experimentally measured phase differences.

The experimental stimulus set with 3 different amplitudes and 9 different stimulus rise times was found to provide the largest variation in neuronal responses and thus provide the best test data for distinguishing the two candidate models. As seen in Tables 1 and 2 the recurrent thalamocortical model give better fits for these experiments, i.e., experiments 1–3, than the feedforward model. The increases in the error measure ε (Eq. 22) for the feedforward model compared to the recurrent model are between 20% and 60%. The results for the thalamocortical transfer in experiment 1 shown in Fig. 9 indicate that the apparent superiority of the recurrent models mainly lies in its ability to account for the rapidly varying parts of the measured layer-4 population response. As seen in the lower left panel of this figure, the ratio of the frequency contents of the experimentally extracted layer-4 and thalamic signals (solid line) is better accounted for by the recurrent model (red line) than the feedforward model (blue line) for frequencies above 20 Hz. For frequencies below 20 Hz the difference is less. For experiment 2, where the increase in error from the recurrent to the feedforward model is even larger, this tendency is even more pronounced (data not shown).

Thalamocortical impulse response. Another traditional dynamical systems measure is the *impulse-response function*, i.e., the response to a very brief input signal [30]. Fig. 10 shows the impulse response of the recurrent thalamocortical model (Eq. 2) with model parameters fitted to experiment 1, cf. Table 1. In this
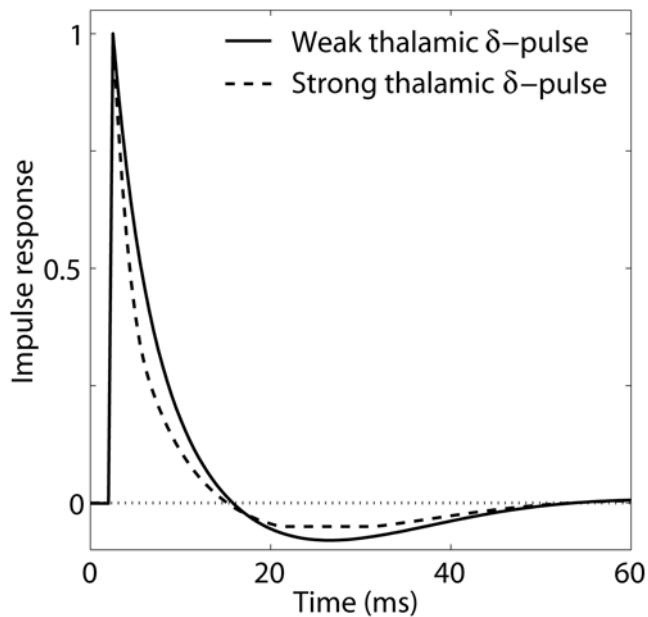
Figure 10. Thalamocortical impulse response for experiment 1. Impulse response for thalamocortical recurrent model (Eq. 2), i.e., additional response due to sharp 'δ-function'-like impulse, 'δ-pulse', of extra thalamic firing superimposed on the steady-state thalamic background activity. The parameter values from fitting to experiment 1 are used (cf. Table 1). The steady-state thalamic firing is set to corresponds to a steady-state layer-4 input 'current' $I_4 = 0.02$, i.e., on the linear flank of the layer-4 activation function (cf. Fig. 4). Solid line corresponds to a linear impulse response, i.e., response to a sufficiently weak δ-pulse so that only the linear part of the activation $F_4(I_4)$ is encountered. Dashed line corresponds to a strong δ-pulse of extra thalamic firing resulting in a maximum value of $I_4 = 0.89$, i.e., far into the non-linear region of the activation function.
doi:10.1371/journal.pcbi.1000328.g010

context the impulse response is the additional evoked firing in the layer-4 population when adding a sharp impulse, 'δ-pulse', to the background thalamic input. The solid line represents the impulse response for a background activity corresponding to the linear flank of the activation function $F_4(I_4)$ where the strength of the δ-pulse is so small that the circuit remains in the linear regime. The observed impulse response is biphasic with an excitatory phase lasting about 15 ms followed by an inhibitory phase lasting up to 50 ms. The dashed line shows the response to a very strong δ-pulse so that the nonlinear regions of the activation function, both the parabolic and half-wave rectifying parts, are encountered. The response to this strong excitation is seen to be qualitatively similar to the linear impulse response. However, the excitatory phase is somewhat sharper, and the long inhibitory phase is modified by the half-wave rectification imposed by the requirement of nonnegative firing rates.

The biphasic thalamocortical impulse-response observed in Fig. 10 qualitatively resembles the temporal shape (i.e., excitation followed by suppression) of the 'impulse-response' to single whisker flicks observed in about two thirds of the barrel-cortex neurons in a single-unit study of Webber and Stanley [33]. The remaining third of the neurons in this study was found to have a second excitatory phase following the suppression [33]. It should be noted, however, that this 'stimulus-cortical' impulse-response is different from the thalamocortical impulse-response extracted here, since the 'stimulus-cortical' response also incorporates the processing between the whisker and the thalamus. A second excitatory phase in the 'stimulus-cortical' impulse response could thus be compatible with

the observed biphasic thalamocortical impulse-response if the thalamic response to a single whisker flick has two temporally distinct positive phases (f.ex., due to cortical feedback onto the thalamic neurons).

Intracortical model

Layer 4 is generally thought of as the dominant input layer for sensory activation of cortex. The supragranular population of layer-2/3 pyramidal neurons appears to receive a dominant input from the layer-4 population, and the initial stimulus-evoked response in layer 2/3 appears to largely stem from layer 4 neurons which in turn are activated by the thalamic input [11,34–41]. We thus investigated models that could account for the experimentally extracted population firing-rate of the layer-2/3 population with the extracted layer-4 population rate as input. We initially described this activity using a combined feedforward and recurrent model analog to Eq. (1), i.e.,

$$r_{2/3}(t) = F_{2/3}([(\beta_{Ef}h_{Ef} - \beta_{If}h_{If}) * r_4](t) + [(\beta_{Er}h_{Er} - \beta_{Ir}h_{Ir}) * r_{2/3}](t)) \tag{10}$$

This form assumes that the interlaminar connections from layer 4 to layer 2/3 are predominantly provided by the excitatory neurons [38]. Fitting of this form to the experimental data revealed that the extracted population firing rates can be explained with a strongly reduced version incorporating only the excitatory feedforward term in Eq. (10), i.e.,

$$r_{2/3}(t) = F_{2/3}([\beta_{Ef}h_{Ef} * r_4^x](t)) \tag{11}$$

As before the weight β_{Ef} was set to unity without loss of generality. Further, the feedforward delay Δ_{Ef} was found to be very small and consequently set to zero. Table 3 and Fig. 11 (upper row) show the results of fitting this model to the experimentally extracted layer-2/3 firing rates $r_{2/3}^x$ using the layer-4 firing rate r_4^x as input for experiments 1–3. A first observation is that the simple model in Eq. (11) accounts excellently for the experimental data; the error is less than 0.03 for all experiments. The fitted time constants τ_{Ef} are all very short, less than 2 ms. The fitted activation functions for experiments 1 and 2 have significant non-linear, i.e., parabolic, contributions with shorter linear flanks than the corresponding activation functions for the recurrent thalamocortical model.

A strong feedforward connection between the layer-4 and layer-2/3 populations is in accordance with previous experimental studies [34–36], and also with the results from the joint modeling of the present MUA data and the corresponding LFP data using *laminar population analysis (LPA)* in Einevoll et al. [11]. However, this LPA analysis also indicated a recurrent interaction within layer 2/3, in accordance with experimental observations by Feldmeyer et al. [42] of a substantial connectivity between layer-2/3 pyramidal neurons. Such a recurrent connection between excitatory neurons could amplify synchronous feedforward excitation from layer 4 [42]. In the present modeling study we find that no such excitatory recurrent terms are needed to account for the present stimulus-evoked experimental data. Instead the stronger inputs are amplified in our model by means of the boosting nonlinearity inherent in the activation function $F_{2/3}(\cdot)$, cf. Fig. 11. We therefore investigated to what extent recurrent connections, i.e., a model of the recurrent form in Eq.
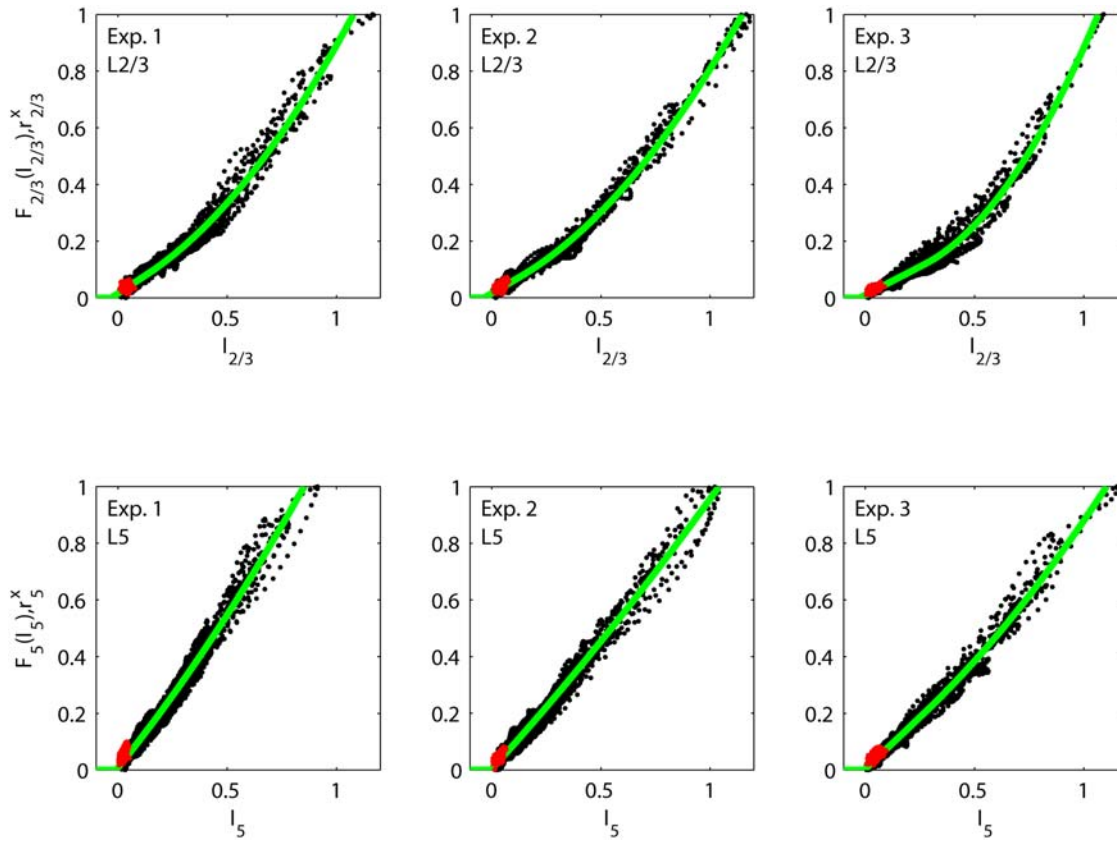
Figure 11. Fits of intracortical model. Illustration of fits of the intracortical model (Eq. 11) to data from experiments 1–3. Each dot corresponds to the experimentally measured layer-2/3 firing rate $r^x_{2/3}(t_i)$ (upper row) or layer-5 firing rate $r^x_5(t_i)$ (lower row) at specific time points t_i plotted against the fitted model values of $I_{2/3}(t_i)$ or $I_5(t_i)$, respectively. The red dots are the corresponding experimental data points taken from the first 5 ms after stimulus onset (for all 27 stimuli). These data points show the activity prior to any stimulus-evoked thalamic or cortical firing and represent background activity. The solid green curves correspond to the fitted model activation functions $F_{2/3}(I_{2/3})$ (upper row) and $F_5(I_5)$ (lower row), respectively.
doi:10.1371/journal.pcbi.1000328.g011

(10) with $\beta_{If} = 0$, improved the fit for the situation with a *linear* activation function. In our test runs, it did not. For experiment 1 with linear activation function the error was found to only be reduced from $\varepsilon = 0.051$ to $\varepsilon = 0.046$ when adding recurrent excitation and inhibition. In comparison, the error for the simple feedforward model with a non-linear activation function was found to be only 0.021, cf. Table 3.

We also investigated to what the extent the extracted layer-5 population firing rate can be accounted for by the same type of firing-rate model with the layer-4 population providing the stimulus-evoked input [43,44]. Table 3 and Fig. 11 (lower row) show the results of fitting a model of the type in Eq. (11) to the experimentally extracted layer-5 firing rates r^x_5 using the layer-4 firing rate r^x_4 as input for experiments 1–3. Again we observed that the simple feedforward model accounts excellently for the experimental data with an error of less than 0.02 for all experiments. The fitted time constants τ_{Ef} are again short, less than 3 ms. The most striking difference from the fits of the layer-5 firing rate is the almost linear activation functions. Thus the layer-5 firing rate appears to be related to the layer-4 firing rate in a very simple manner for the present experimental situation.

The presently extracted intracortical models have very simple mathematical forms. For example, for the layer-4 to layer-2/3 transfer the model on integral form can be translated to a simple

differential equation using the 'linear-chain trick' as described in Materials and Methods, i.e.,

$$\tau_{Ef} \frac{dx_{2/3}}{dt} = -x_{2/3} + r_4(t) \qquad (12)$$

where the layer-2/3 firing rate is given by $r_{2/3}(t) = F_{2/3}(x_{2/3}(t))$. The same type of differential equation is found for the connection between layer 4 and layer 5 (with $x_{2/3}(t)$ substituted by $x_5(t)$ in Eq. (12)). In this case the signal transfer is essentially described by a simple linear differential equations for $r_5(t)$ since $r_5(t) = F_5(x_5(t)) \simeq a_5 x_5(t)$.

Intracortical transfer

We next investigated the intracortical transfer functions. The linear transfer function from the layer-4 population to the layer-2/3 and layer-5 populations is found from Eq. (11) to be given by

$$T_{n/4}(\omega) = \tilde{r}_n(\omega)/\tilde{r}_T(\omega) = F_n^{'}(I_{n0})\tilde{h}_{Ef}(\omega) = \frac{F_n^{'}(I_{n0})}{1 - i\tau_{Ef}\omega} \qquad (13)$$

where n represents 2/3 or 5, and $\tilde{h}_{Ef}(\omega)$ is found in Eq. (39). This corresponds to a low-pass filter, i.e., no resonance behavior as for

Table 3. Fitted model parameters for intracortical models.

L4→L2/3	Exp. 1	Exp. 2	Exp. 3
τ_{Ef} (ms)	1.2	1.2	1.8
$a_{2/3}$	0.51±0.01	0.45	0.40
$b_{2/3}$	0.49±0.01	0.45	0.89
$I_{2/3}^{\dagger}$	−0.03	−0.03	−0.02
$I_{2/3}^{*}$	0.13±0.02	0.13	0.27
error (ε)	0.0214	0.0141	0.0279
L4→L5	**Exp. 1**	**Exp. 2**	**Exp. 3**
τ_{Ef} (ms)	3.0	2.1	1.4
a_5	0.96	0.86±0.01	0.73
b_5	0.24	0.10	0.27
$I_5^{\dagger}$	−0.009	−0.003	−0.004
I_5^{*}	0.003	0.024±0.043	0.268±0.004
error (ε)	0.0195	0.0193	0.0167

Resulting optimized parameters for the intracortical network model (Eq. 11) for experiments 1–3. Upper row: Layer-2/3 firing rate predicted from layer-4 input. Lower row: Layer-5 firing rate predicted from layer-4 input (where the subscripts '2/3' are replaced by '5' in Eq. (11)). The listed parameter values correspond to the mean of estimated parameters from 25 selected models giving essentially the same error (see Materials and Methods). The standard deviations are only listed if they exceed the last digit of the mean.
doi:10.1371/journal.pcbi.1000328.t003

the recurrent thalamocortical model in Eq. (9). Further, the impulse-response function is the simple (monophasic) exponentially decaying function, contrasting the biphasic thalamocortical impulse-response functions seen in Fig. 10.

In Fig. 12 we compare predictions for the transfer ratio from this simple linear feedforward model using the fitted parameters from Table 3 with the corresponding experimental result $r_n^x(\omega)/r_4^x(\omega)$ ($n=2/3$ or 5) for six of the stimulus conditions providing the strongest cortical responses in experiment 1 ($a3,t1; a3,t2; a3,t3; a2,t1; a2,t2; a2,t3$). For the layer-5/layer-4 transfer ratio (lower row in Fig. 12) we see an excellent agreement between experiments and linear theory. This is as expected since the fitted layer-5 activity functions $F_5(\cdot)$ are essentially linear (cf. Fig. 11). For the transfer ratio between layer 2/3 and layer 4 a more substantial deviation between the experimental and linear-model transfer rations is observed, in particular a slightly growing transfer-ratio amplitude for large frequencies. This deviation presumably reflects the non-linearities of the layer-2/3 activity functions $F_{2/3}(\cdot)$, because the same effect is also observed for the transfer ratio between the best model fit $r_{2/3}$ and r_4^x (cf. red line in upper left panel of Fig. 12).

Discussion

A main objective of the present paper is the description and application of a new method for extraction of population firing-rate models for thalamocortical and intracortical signal transfer on the basis of trial-averaged data from simultaneous cortical recordings with laminar multielectrodes in a rat barrel column and single-electrode recordings in the homologous thalamic barreloid. Below we first discuss the results from the model estimation for both the thalamocortical and the intracortical signal transfer, followed by a discussion of the model estimation method itself.

Thalamocortical models

For the thalamocortical signal transfer our investigations clearly identifies a model with (1) fast feedforward excitation, (2) a slower predominantly inhibitory process mediated by recurrent (within layer 4) and/or feedforward interactions (from thalamus), and (3) a mixed linear-parabolic activation function. The relative importance of the feedforward compared to the recurrent connections is more difficult to determine and has been a subject of significant interest [7–9,16,45]. Here we have compared two alternative models: (i) a purely *feedforward* thalamocortical model with feedforward excitation and inhibition and (ii) a *recurrent* model with feedforward excitation, recurrent excitation and recurrent inhibition (but no feedforward inhibition). In reality the inhibitory layer-4 neurons receive excitatory inputs both from thalamic neurons and other layer-4 neurons, and the inhibition felt by the excitatory layer-4 neurons will thus be both 'feedforward' and 'recurrent'; the different models thus explore what part appears to dominate in the present experimental situation.

Our results suggest that the model with recurrent inhibition better accounts for the present experimental data than the model with feedforward inhibition, i.e., that the layer-4 interneurons providing the inhibition of the layer-4 excitatory neurons are in turn mainly driven by excitation from layer-4 neurons. Since the relative strength of recurrent effects compared to feedforward effects appears to increase with increasing thalamic stimuli [19], this might indicate that the present fits to the experimental data is dominated by 'strong' inputs. Alternatively, it may be that a strong feedforward inhibition is also present, but that it is strongly overlapping in time with the feedforward excitation. Then the present modeling scheme and experimental data are unable to separate them and instead lump the effect of this inhibition together with the feedforward excitation.

An interesting result from the present investigation is that we find a similar thalamocortical population model as Pinto et al. [8,9]: the *recurrent* model on integral form in Eq. (2) can be mapped to a set of two differential equations (Eqs. 4–5) structurally similar to the model suggested and investigated by Pinto and coworkers. The correspondence between the behavior of these models is demonstrated by the phase-plane plots in Fig. 5, which exhibits the same qualitative features as the analogous phase-plane plots in Ref. [9]. This close correspondence is striking since the methods used to derive the models are very different. Pinto et al. chose the model to account for a large collection of single-unit PSTHs recorded with sharp electrodes from numerous animals. By contrast, our model parameters were extracted based on simultaneous thalamic and cortical recordings from individual animals. As multielectrode arrays allow for convenient simultaneous recordings from all layers of the cerebral cortex, even at more than one cortical location [10], the proposed modeling approach scales more readily to complex networks involving multiple, spatially separated, neuronal populations.

Intracortical model

The presently identified intracortical model for the connection between the layer-4 and layer-2/3 populations has a very simple mathematical form including only a single feedforward term (Eqs. 11–12), but was nevertheless found to account excellently for the experimental data, cf. Fig. 11. Such a strong feedforward connection between these populations is in accordance with previous experimental studies [34–36]. An experimental study by Feldmeyer et al. [42] found substantial recurrent connectivity between layer-2/3 pyramidal neurons, but no such excitatory recurrent terms were needed to account for the present stimulus-evoked experimental data. Compared to the thalamocortical
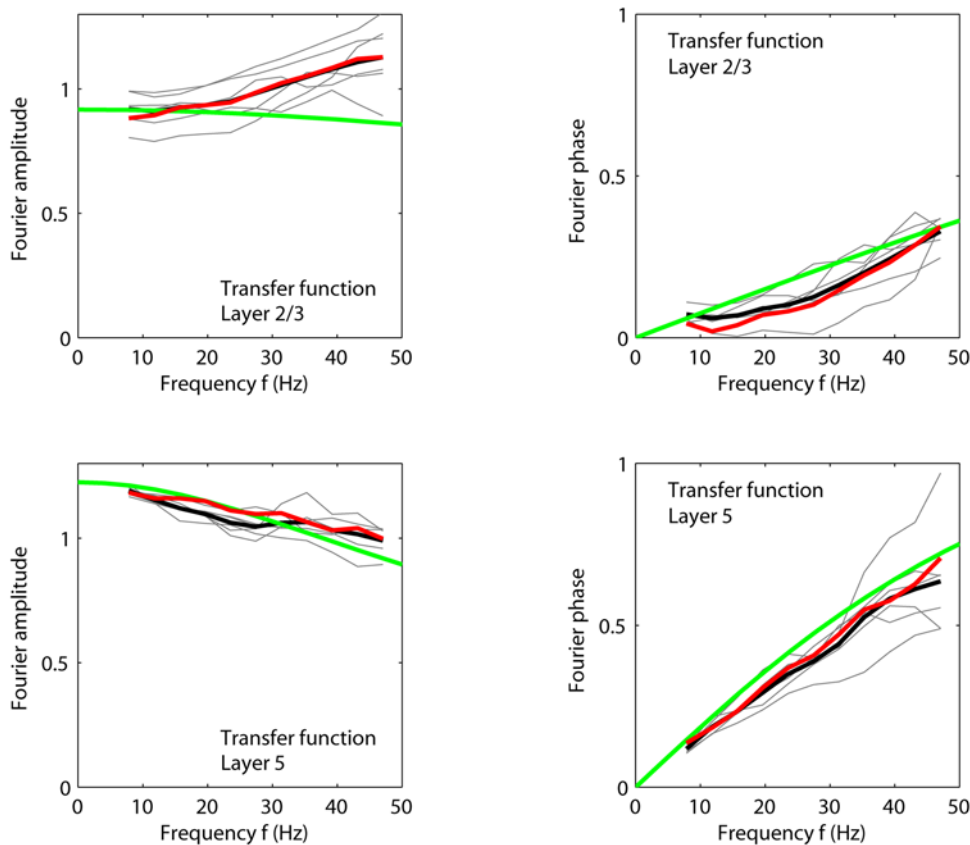
Figure 12. Intracortical transfer for experiment 1. Transfer ratios $r_n^x(2\pi f)/r_4^x(2\pi f)$ for six stimulus conditions providing the strongest response ($a3,t1$; $a3,t2$; $a3,t3$; $a2,t1$; $a2,t2$; $a2,t3$) are shown as thin grey lines. (Note that $f = \omega/(2\pi)$.) Thick black lines represent the corresponding averages for the six stimuli. Upper left: Transfer to layer 2/3, amplitude. Upper right: Transfer to layer 2/3, phase. Lower left: Transfer to layer 5, amplitude. Lower right: Transfer to layer 5, phase. Examples of model predictions from the linearized intracortical transfer-function model in Eq. (13) are shown (dashed lines) for the parameter values corresponding to the fitted values of τ_{Ef} and Δ_{Ef} for experiment 1 taken from Table 3. The work-point derivatives were chosen to be $F'_{2/3}(I_{2/3} = 0.55) = 0.92$ and $F'_5(I_5 = 0.55) = 1.22$, respectively. The red lines correspond to the average of the amplitude (left panels) and phases (right panels) of the transfer ratios found for the six stimuli listed above when driving the fitted feedforward intracortical layer-2/3 and layer-5 models of the type in Eq. (11) with the experimentally extracted layer-4 input $r_4^x(t)$.
doi:10.1371/journal.pcbi.1000328.g012

transfer, the intracortical transfer displayed limited variation for the present set of stimuli under the present experimental conditions. The absence of identified recurrent terms in our intracortical models may thus be due to lack of sufficient variance in the experimental data to allow for identification of such a model term. Instead recurrent intracolumnar interactions in layer-2/3 may be involved in shaping the non-linear activation function $F_{2/3}(\cdot)$ and thus modifying the dynamics in a way which cannot be accounted for by the present recurrent model with a linear activation function.

As seen in Fig. 11 and Table 3 a simple feedforward model can, based on the layer-4 population firing rate, also account excellently for the observed layer-5 population firing rate. As for the layer-4 to layer-2/3 pathway, the fitted time constants are quite short, 3 ms or less. Interestingly, the fitted activation function is found to be almost linear ($r_5 \simeq a_5 x_5$, cf. (12)), so that the dynamics of the layer-5 population firing rate can be described simply by $\tau_{Ef} dr_5/dt = -r_5 + a_5 r_4$. Monosynaptic connections between pairs of spiny stellate cells in layer 4 onto the basal dendrites of layer-5 pyramidal cells compatible with a such a fast feedforward connection have been observed experimentally [43,44]. Moreover, results from the LPA analysis of the present data in Einevoll et al. [11] were compatible with such an excitatory synaptic connection from layer 4 onto the basal layer-5 neuron

dendrites. However, the presently extracted intracortical firing-rate model may simply reflect that extracted firing rates for the cortical populations are strongly overlapping in time. An alternative explanation for the observed tight temporal correlation between the layer-4 and layer-5 firing rates could be correlations between the input from thalamic neurons in VPM onto layer 4 with VPM inputs to layer-5B neurons [46] and/or 'paralemniscal' input via POm to layer 5A neurons [39,47]. Thus while the thalamocortical transfer seems to be well probed by the present stimulus paradigm, i.e., the set of stimuli provides a varied set of paired thalamic and layer-4 responses, this is less so for the intracortical transfer. One should thus search for other experimental paradigms to probe the intracortical population-rate dynamics further.

As a methods test we also investigated to what extent our feedforward model could account for the 'backwards' connections, i.e., whether the layer 4 firing could mathematically be accounted for by the model in Eq. (11) with the extracted layer-2/3 or layer-5 population firing rates as input respectively. These connections are expected to be weak [37,41], and indeed, since the layer-4 firing initiates somewhat earlier than the rest of the laminar populations, the best fits were found for unrealistically small time constants ($\tau_{Ef} < 0.1$ ms). The model solutions naturally failed to predict the onset of the layer-4 firing correctly, indicating their inadequacy.

Coding properties of thalamocortical and intracortical circuits

A conclusion from our study is that the signal processing in the thalamocortical and intracortical circuits is very different. The thalamocortical circuit favors rapid whisker movements in that sharply rising thalamic population firing rates evokes large cortical responses. For such stimuli the fast excitation in the circuit dominates the slower, but eventually stronger, inhibition at short time scales thus ensuring a large population firing-rate in the layer-4 population for a certain time window. For slower whisker movements the inhibition overtakes the excitation before a strong cortical response has emerged. This essential feature is demonstrated by the phase-plane plots in Fig. 5. In frequency space the effect translates into a resonance-like amplification of the transfer function at intermediate frequencies ($\sim$15–20 Hz), cf. Fig. 9, while the impulse response function is biphasic, cf. Fig. 10. In terms of coding the thalamocortical transfer can be said to map time derivatives of the thalamic population firing rate onto amplitudes in the population firing of cortical layer 4 [9,16]. Thus the thalamocortical circuit is sensitive to angular whisker velocity, explaining why a rich variety of cortical responses are observed for the stimulus set with three different amplitudes and nine different rise times.

The intracortical circuits appear very different. Here the extracted models perform low-pass filtering, but the time constants are so short, typically 1–3 ms, that the cutoff frequency is large: for firing-rate frequencies up to 50 Hz only modest reductions in the transfer ratio is observed, cf. Fig. 12. In contrast to the typical biphasic form seen for the impulse response for the thalamocortical model in Fig. 10, the impulse response of the intracortical models is a rapid exponentially decaying (monophasic) function. Thus, while the thalamus to layer-4 circuit appears to selectively respond to synchronous inputs with large time derivatives, the layer-4 to layer-2/3 circuit appears to perform a simple amplitude mapping [16].

Current limitations and potential future extensions

A core assumption in our modeling scheme is that the MUA signal is proportional to the population firing rate [48,49]. This assumption was recently investigated by Pettersen et al. [12] in a forward-modeling study of extracellular potentials from a population of layer-5 pyramidal cells from cat visual cortex receiving synchronous synaptic activation resembling the present stimulus-evoked situation. For *trial-averaged* data a roughly linear relationship was observed for a large range of small and intermediate population firing rates. For large population firing rates the true population firing rate was found to grow super-linearly with the MUA due to increasing cancelation of extracellular potentials for high firing rates. It is, however, unclear whether or to what extent such a superlinear relationship can be expected here.

A number of factors in our study could affect the magnitude and frequency content of the recorded electrophysiological response in comparison with awake behaving animals in a natural environment. Among them are anesthesia conditions and the use of an artificial single-whisker stimulus in the absence of active whisking. The present study used alpha-chloralose, an anesthetic agent used widely in neurophysiological and hemodynamic studies due to its lesser effects on cardiovascular, respiratory and reflex functions [50–52]. Qualitatively similar laminar profiles of evoked MUA response was observed with ketamine [11], but a systematic study is needed to investigate the effects of anesthesia on the identified network models.

Presently we have assumed the measured MUA to correlate with the excitatory population. Due to their lower neuron numbers the inhibitory populations are expected to contribute less, although differences in morphology and firing rates between excitatory and inhibitory neurons will also affect their relative contributions [13]. More forward-modeling studies along the lines of Pettersen et al. [12] are needed to investigate this relationship between the measured MUA and the underlying neural activity in intermixed excitatory and inhibitory populations.

In the current models only the firing rates of the excitatory laminar populations are modeled explicitly, while the inhibitory neurons are merely considered to modify the dynamics of, and interaction between, these excitatory populations. An alternative to the single population Volterra firing-rate model for the thalamocortical transformation in Eq. (1) could be the following generalization including an explicit dynamical equation also for the inhibitory firing rate, i.e.,

$$
\begin{aligned}
r_{\mathrm{E4}}(t) &= F_{\mathrm{E4}}(I_{\mathrm{E4}}) \\
&= F_{\mathrm{E4}}(\alpha_{\mathrm{TE}}[h_{\mathrm{TE}} * r_{\mathrm{T}}](t) + \alpha_{\mathrm{EE}}[h_{\mathrm{EE}} * r_{\mathrm{E4}}](t) - \alpha_{\mathrm{IE}}[h_{\mathrm{IE}} * r_{\mathrm{I4}}](t))
\end{aligned}
\tag{14}
$$

$$
\begin{aligned}
r_{\mathrm{I4}}(t) &= F_{\mathrm{I4}}(I_{\mathrm{I4}}) \\
&= F_{\mathrm{I4}}(\alpha_{\mathrm{TI}}[h_{\mathrm{TI}} * r_{\mathrm{T}}](t) + \alpha_{\mathrm{EI}}[h_{\mathrm{EI}} * r_{\mathrm{E4}}](t) - \alpha_{\mathrm{II}}[h_{\mathrm{II}} * r_{\mathrm{I4}}](t))
\end{aligned}
\tag{15}
$$

This model explicitly includes thalamic input to both the excitatory and inhibitory populations as well as all possible recurrent connections [9]. The two integral equations in Eqs. (14–15) can be mapped to a set of four differential equations using the 'linear-chain trick' [14]. However, as shown in Materials and Methods, the model in Eqs. (14–15) can be reduced to our model in Eq. (1) under the assumptions that (1) the inhibitory firing-rate function is linear, i.e., $F_{\mathrm{I4}}(I) = a_{\mathrm{I4}}I$, (2) the self inhibition is zero, $\alpha_{\mathrm{II}} = 0$ [53], and (3) by making the identifications $\alpha_{\mathrm{TE}} h_{\mathrm{TE}} \rightarrow \beta_{\mathrm{Ef}} h_{\mathrm{Ef}}$, $a_{\mathrm{I4}} \alpha_{\mathrm{IE}} \alpha_{\mathrm{TI}} h_{\mathrm{TI}} * h_{\mathrm{TI}} \rightarrow \beta_{\mathrm{If}} h_{\mathrm{If}}$, $\alpha_{\mathrm{EE}} h_{\mathrm{EE}} \rightarrow \beta_{\mathrm{Er}} h_{\mathrm{Er}}$, and $a_{\mathrm{I4}} \alpha_{\mathrm{IE}} \alpha_{\mathrm{EI}} h_{\mathrm{IE}} * h_{\mathrm{EI}} \rightarrow \beta_{\mathrm{Ir}} h_{\mathrm{Ir}}$, cf. Eqs. (43–47).

The analysis of model parameter identifiability revealed that certain linear combinations of parameters (notably recurrent and feedforward excitation and inhibition strengths, time constants, and activation function parameters), do not have a measurable effect on the measured signals, and thus cannot be confidently estimated. This problem can be partly addressed by using intracellular recordings to measure some of these parameters, e.g., synaptic time constants and firing rates as function of somatic input currents, directly in the relevant cell types. Model identification could also be aided by theoretical investigations of the basic structure of population firing-rate models [54,55].

Furthermore, intercolumnar signal propagation can be modeled through connecting single-column firing-rate models of the present type based on known connectivity between neighboring columns or commissural projections [56–62]. Such multicolumn models may provide insights into the mechanisms of more complex cortico-cortical interactions such as surround [63,64] and transcallosal inhibition in SI [65–67].

Several groups have attempted to derive information about functional connectivity between cortical areas based on non-invasive imaging data [68,69]. A further development of this approach, aimed at providing a general theory of information processing in hierarchies of cortical areas, has recently been proposed by Friston [70,71]. The interpretation of the results from such high-level modeling approaches has been limited by the lack of a biophysical measurement theory relating the imaging signals

to the underlying neuronal population activity and the connections between neuronal populations. The modeling approach described here could provide the necessary biophysical grounding for such theories, as the noninvasive electroencephalography (EEG) and magnetoencephalography (MEG) signals can be directly predicted based on the laminar distribution of current sources and sinks, along with information about the geometry of the cortical surface of the individual subject [72,73]. Thus, by embedding the proposed 'mesoscopic' modeling approach within a macroscopic modeling framework, such as the Hierarchical Dynamical Model (HDM) proposed by Friston [71], it may ultimately be possible to bridge the gap from the cellular to the systems-level of description, and from invasive to non-invasive recordings.

Materials and Methods

Experimental procedure

All experimental procedures were approved by the Massachusetts General Hospital Subcommittee on Research Animal Care. Male Sprague-Dawley rats (250–350 g, Taconic) were used in the experiments. Glycopyrrolate (0.5 mg/kg, i.m.) was administered 10 minutes before the initiation of anesthesia. Rats were anesthetized with 1.5% halothane in oxygen for surgery. Following surgery (see below), halothane was discontinued, and anesthesia was maintained with 50 mg/kg intravenous bolus of alpha-chloralose followed by continuous intravenous infusion at 40 mg/kg/h. During surgery a tracheotomy was performed, cannulae were inserted in the femoral artery and vein. All incisions were infiltrated with 2% lidocaine. Following tracheotomy, rats were mechanically ventilated with 30% O_2 in air. Ventilation parameters were adjusted to maintain the following blood gas readings: $PaCO_2$ between 35 and 45 mm Hg, PaO_2 between 140 and 180 mm Hg, and pH between 7.35 and 7.45. Heart rate, blood pressure, and body temperature were monitored continuously. Body temperature was maintained at $37.0\pm0.5°C$ with a homeothermic blanket (Harvard Apparatus, Holliston, MA, USA). The animal was fixed in a stereotaxic frame. An area of skull overlying the primary somatosensory cortex was exposed and then thinned with a dental burr. The thinned skull was removed and the dura matter dissected to expose the cortical surface. A barrier of dental acrylic was built around the border of the exposure and filled with saline.

Mapping with a single metal microelectrode (FHC, 2–5 MΩ) was done to determine the positioning of the linear (laminar) multielectrode array in barrel cortex. The optimal position was identified by listening to an audio monitor while stimulating different whiskers. Following the mapping procedure, the electrode was withdrawn, and the laminar electrode was slowly introduced at the same location perpendicular to the cortical surface. Contact no. 1 was positioned at the cortical surface using visual control with saline covering the exposed cortex around the laminar electrode. The linear multielectrode had 23 contacts with diameter 0.04 mm spaced at 0.1 mm [49], and data from contacts 2 to 23 was used in the further analysis.

The thalamic recordings were performed using single metal microelectrodes (FHC, 5–7 MΩ). The ventral posteriomedial thalamic nucleus (VPM) was targeted using stereotactic coordinates (VPM: AP −3.6 to −3.0, ML 2.0 to 3.5, DV 5.0 to 7.0). VPM (rather than POm) was chosen because it provides the dominant input to cortical layer 4 [74].

Single whiskers were deflected upward by a wire loop coupled to a computer-controlled piezoelectric stimulator. The stimulus sequence was optimized using the approach described by Dale [75]. This method optimizes efficiency for Finite Impulse

Response (FIR) estimation, and, thus, makes no a priori assumption of the response shape. Stimuli were presented at a fixed rate of one per second, with 25% of stimuli being 'null events' (zero amplitude whisker flicks). The method was used to optimize the order of stimulus conditions so as to optimize estimation efficiency of the event-related neuronal responses. We used two stimulus conditions: In the first stimulus condition, with altogether 27 different stimuli, three stimulus amplitudes (vertical displacements 0.40 mm ($a1$), 0.80 mm ($a2$), and 1.2 mm ($a3$)) each with nine stimulus rise times (20 ms ($t1$), 30 ms ($t2$),…, 100 ms ($t9$)) were applied. The stimulus angular velocity varied between 76 deg/s ($a1,t9$) and 1090 deg/s ($a3,t1$). In the second stimulus condition a fixed stimulus rise time (time from onset to maximum displacement) of 30 ms was used, with 27 different, linearly incrementing, vertical displacements up to 1.2 mm (amplitude 27).

Preprocessing of experimental data

The recorded laminar-electrode potential was amplified and analogically filtered online into two signals: a low-frequency part and a high-frequency part [49]. Only the high-frequency part (150–5000 Hz, sampled at 20 kHz with 12 bits) was used in the present analysis. This signal was further filtered digitally between 750 Hz and 5000 Hz using a zero phase-shift second-order Butterworth filter, and then *rectified* along the time axis to provide the multi-unit activity (MUA). This non-negative high-frequency 'envelope' reflects firing of action potentials [12,48,49]. The time-resolution of this MUA signal was then decimated by a factor 10, reducing the time resolution of the data from 0.05 ms to 0.5 ms [11].

Sample traces of the laminar-electrode MUA (prior to rectification) for a single trial can be seen in Figure 1B in Einevoll et al. [11]. The process of (1) band-pass filtering (750–5000 Hz), (2) rectification, and (3) decimation was also applied to the thalamic single-electrode recordings to provide the thalamic MUA signal. The presently used *trial-averaged* data were obtained by averaging over all 40 trials for each stimulus type.

Six experiments recorded from a total of three rats were considered. In experiments 1–3 the stimulus condition with 3 amplitudes and 9 rise-times was used, while the 27-amplitude stimulus condition was used in experiments 4–6. Experiments 1, 2, 4 and 5 were from a single rat, while experiments 3 and 6 were from two other rats. About ten (out of 6480) trials were removed due to artifacts in the laminar-electrode MUA. In experiments 3 and 6, the laminar-electrode MUA signal from contact no. 9 was erratic; for this channel the arithmetic mean of the MUA signals from the neighboring contacts (contacts no. 8 and 10) was therefore used instead. The trial-averaged MUA data used for the estimation of cortical population firing rates is denoted $\Phi_M(z_i,t_j)$. z_i and t_j refer to the electrode position and time, respectively, and the indices i and j run over electrode contacts and time points.

Estimation of thalamic population firing rate

The MUA recorded by the single thalamic electrode was used as a measure of the population firing rate of thalamic neurons in a barreloid in VPM projecting onto the homologous barrel. An estimate of the trial-averaged thalamic firing rate $r_T^x(t)$ was found by an additional low-pass filtering of the MUA using a zero phase-shift, third order Butterworth filter with a cutoff frequency of 200 Hz. With this filter a δ-function is transformed to a peak with a half-width of about 2 ms. The value of the resulting rate signal was then shifted and normalized in each experimental data set separately so that the minimum and maximum estimated

(normalized) thalamic firing rate over all times and stimulus conditions was zero and unity, respectively.

Estimation of cortical population firing rates

The estimation of population firing rates of laminar cortical populations from laminar-electrode MUA is less straightforward. However, Einevoll et al. [11] recently developed a new method, *laminar population analysis (LPA)*, for analysis of laminar-electrode data. Using this method, laminarly organized neuronal populations can be identified and the time dependence of the population firing rates estimated. The laminar-electrode MUA data $\Phi_M(z_i, t_j)$ are then modeled as a sum over spatiotemporally separable contributions from several neuronal populations, i.e.,

$$\Phi_M^m(z_i, t_j) = \sum_{n=1}^{N_{pop}} M_n(z_i) m_n(t_j) \tag{16}$$

where N_{pop} is the number of populations, $M_n(z)$ is the MUA spatial profile related to firing of action potentials in neuronal population n, and $m_n(t)$ relates directly to the corresponding time course of firing activity in this population. With additional physiological constraints imposed on the general shape of $M_n(z)$, both $M_n(z)$ and $m_n(t)$ can, as described in Einevoll et al. [11], be determined in an optimization scheme minimizing the square deviation between $\Phi_M^m(z_i, t_j)$ and the experimental data $\Phi_M(z_i, t_j)$. In Einevoll et al. [11] four distinct cortical populations were identified and putatively interpreted as layer 2/3, layer 4, layer 5, and layer 6 (and/or deep layer 5) populations. Experiments 1, 3, 5, and 6 correspond to data also analyzed there, and fitted results for $m_n(t)$ from this study were applied directly. For illustration of the correspondingly estimated spatial profiles $M_n(z)$, see Fig. 12 in Ref. [11]. For experiments 2 and 4 new LPA analyses were carried out to extract $m_n(t)$.

Pettersen et al. [12] recently investigated the relationship between action-potential firing in a neuronal population and the MUA recorded by adjacent laminar electrodes. With a forward modeling scheme they calculated the extracellular potential generated by a columnar population of layer-5 pyramidal cells following synaptic activation resembling the stimulus-evoked situation investigated here. They found that a filtered version of the raw MUA in general gave a good measure of the population firing rate, known exactly in their model situation, for the trial-averaged case. Their study thus support the use of Eq. (16). Further, in their forward-model study a Gaussian filter with a standard deviation of 1 ms was found to be suitable. Presently, the signal was low-pass filtered at 200 Hz with a zero phase-shift, third order Butterworth filter, giving a similar temporal filter width. Fig. 13 demonstrates the effect of this low-pass filtering on example raw MUA thalamic and layer-4 population signals both for a weak ($a1, t9$) and a strong ($a3, t1$) stimulus condition.

The resulting filtered estimates

$$r_n^x(t) = C_R m_n^\sigma(t) \tag{17}$$

were then shifted and the constant C_R adjusted so that in each experimental data set the minimum firing rate was zero and the maximum firing rate unity for each identified cortical population. Here the superscript 'x' denotes that the firing-rate estimates stem from experiment, and the superscript 'σ' denotes that the signal has been low-pass filtered.

We assume that $r_n^x(t)$ ($n=2/3,4,5$) is a measure of the firing rate of laminar populations of excitatory neurons. For example, $r_4^x(t)$ is interpreted as the population firing rate of the excitatory neurons in layer 4 of the barrel column. There will certainly also be contributions to the MUA from the inhibitory neurons, but since more than 80% or neurons in barrel cortex are excitatory [39] and the excitatory and inhibitory neurons in layer 4 have been observed to have firing probabilities with similar size and temporal profile when stimulated by the principal whisker [18], we assume the recorded signal to correlate well with the firing-rate of the excitatory population.

Form of population firing-rate model on integral form

The population firing-rate models are formulated as nonlinear Volterra integral equations [5,14],

$$I_n(t) = \sum_m \left(\beta_{Em}[h_{Em} * r_m](t) - \beta_{Im}[h_{Im} * r_m](t) \right),$$

$$r_n(t) = F_n(I_n(t)) \tag{18}$$

where $h(t)$ is a temporal coupling kernel, and $[h * r](t)$ is the temporal convolution given by

$$[h * r](t) = \int_0^\infty h(s) r(t-s) ds \tag{19}$$

The quantity I_n can be interpreted as net input current entering the somas of neurons belonging to population n. This current is assumed to result from previous firing in all presynaptic populations m (possibly including n itself), with h_{Em} and $h_{Im}(t)$ describing the excitatory and inhibitory effects, respectively, of firing at different times in the past. Presently, the temporal coupling kernels h are modeled as (normalized) delayed decaying exponentials, i.e.,

$$h(t) = e^{-(t-\Delta)/\tau} H(t-\Delta)/\tau \tag{20}$$

where $H(\cdot)$ is the Heaviside unit step function. This kernel is specified by two parameters, the time constant τ and the time delay Δ.

In our model the net input current $I_n(t)$ is converted instantaneously into a population firing rate $r_n(t)$ by means of a nonlinear function $F_n(\cdot)$. Here the following four-parameter class of activation functions is used:

$$F_n(I_n) = \begin{cases} 0 & \text{if } I_n < I_n^\dagger \\ a_n(I_n - I_n^\dagger) & \text{if } I_n^\dagger \leq I_n \leq I_n^* \\ a_n(I_n - I_n^\dagger) + b_n(I_n - I_n^*)^2 & \text{if } I_n^* < I_n \end{cases} \tag{21}$$

As illustrated in Fig. 3A this activation function is zero below the threshold $I_n^\dagger$, grows linearly between $I_n^\dagger$ and I_n^*, and quadratically above I_n^*. The activation function is continuous, and the positive coefficients a_n and b_n determine the steepness of the linear and quadratic term, respectively. Note that for $a_n=0$ (or $I_n^\dagger=I_n^*$) the linear part of the activation vanishes. Likewise, for $b_n=0$ (or $I_n^* \rightarrow \infty$) the activation above threshold is linear.

Numerical optimization procedure

The model parameters were estimated by fitting model estimates of the population firing rates $r(t)$ to the corresponding experimentally extracted rates $r^x(t)$ for all stimulus conditions
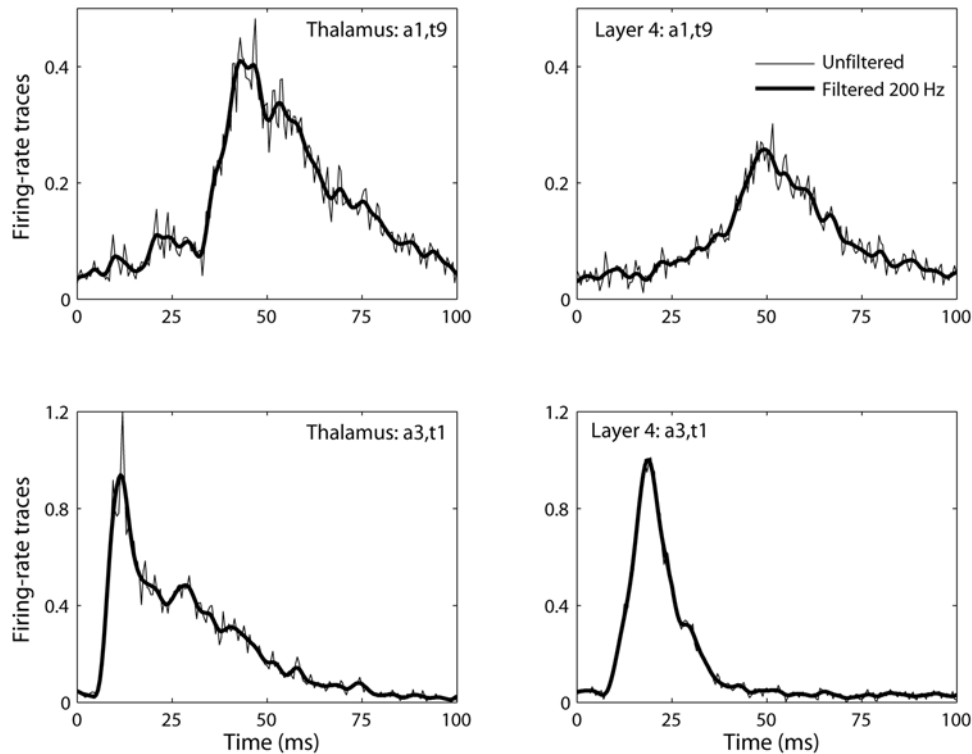
Figure 13. Effects of filtering on population firing-rate estimates. Example trial-averaged firing-rate traces, both unfiltered and filtered, from experiment 1 for the thalamic and layer-4 populations for a weak ($a1,t9$) and a strong stimulus ($a3,t1$). The unfiltered layer-4 traces correspond to $m_4(t)$, cf. Eq. (16), while the layer-4 filtered traces correspond to the firing-rate estimate $r_4^x(t)$ described in Eq. (17). The unfiltered thalamic traces represent the raw single-electrode MUA data. The relationship to the thalamic firing-rate estimate $r_T^x(t)$ is described by Eq. (17).
doi:10.1371/journal.pcbi.1000328.g013

simultaneously. The squared deviation between model and experimental firing rates was used as error measure, i.e.,

$$\varepsilon = \sum_j \varepsilon_j = \sum_j \left(r^x(t_j) - r(t_j)\right)^2 \Big/ \sum_k (r^x(t_k) - \langle r^x \rangle)^2. \quad (22)$$

Here the sums over j and k go over all time steps, i.e., 201 for each stimulus multiplied by the 27 different stimuli, and $\langle r^x \rangle$ denotes the temporal mean of $r^x(t_k)$.

The numerical calculations were done using MATLAB. In the numerical evaluation of the thalamocortical model (Eq. 1) the experimentally extracted thalamic firing rate $r_T^x(t)$ was inserted directly. The convolutions in the feedforward terms on the right hand side of Eq. (1) could thus be performed once and then stored for use in the later numerical procedure. For the recurrent term this is not possible since $r_4(t)$ is evaluated iteratively for each time step. The firing rate r_4 at time t is given by the right hand side of Eq. (1) with the recurrent convolution terms evaluated at time $t - \Delta t$ where $\Delta t = 0.5$ ms is the time step. As a result, the recurrent synaptic connections can be considered to have a fixed time delay of 0.5 ms. The convolutions with the exponential coupling kernels were approximated using MATLAB's FILTER command. No explicit delays were considered for the recurrent terms, but for the feedforward terms delays corresponding to multiples of the time step (0.5 ms) were allowed for.

A three-step optimization procedure was used. In the first step the full model was considered and a preliminary optimization was performed doing a stochastic search starting from several sets of random initial parameter values $\Theta = (\theta_1, \theta_2, \ldots)$ where θ_m represent individual model parameters. We then computed linear correlations between the parameters for an ensemble of fitted models $\{\Theta^*\} = \{(\theta_1^*, \theta_2^*, \ldots)\}$ providing best fits, i.e., lowest values of the error ε in Eq. (22), from this initial search. These correlations were then used to temporarily reduce the number of independent parameters to be used in a second stage of the optimization. For this second stage initial parameter values were chosen randomly from a distribution around the mean parameter values obtained from the ensemble of first-stage fits. After the second round of optimization in the reduced parameter space, all model parameters were again allowed to vary independently in the full parameter space. In this third part of the optimization procedure the initial values were taken to be the parameters resulting from the second-stage run. MATLAB's FMINSEARCH command, based on the Nelder-Mead algorithm, was used at the second and third stages of the optimization procedure. After the establishment of the ensemble of first-stage fits, a set of 25 independent second (and subsequent third) stage optimizations was run. The optimization procedure terminated if all 25 optimization jobs obtained the same minimum error value within 0.0001. If not, the procedure starting from the second stage, was repeated.

Analysis of model 'sloppiness'

In the optimization procedure we take advantage of linear correlations in the ensembles of fitted model parameters. Principal component analysis (PCA) of the covariance matrices $\mathbf{C}$, where $C_{lm} = \langle \langle \theta_l - \langle \theta_l \rangle \rangle \rangle \langle \langle \theta_m - \langle \theta_m \rangle \rangle \rangle$ and $\langle \cdot \rangle$ denotes the ensemble

average, showed a substantial interdependency between these fitted parameters. More than 99% of the variability of the fitted parameters was typically accounted for by the first two components. As a consequence, large variations in the sets of optimal parameters may leave the overall quality of the fit, i.e., the error measure, almost unaffected as long as they are restricted to the subspace spanned by the dominant principal components. This property is called *sloppiness*, and can be quantified by an eigenvalue analysis of the Hessian matrix composed of the partial 2nd derivatives of the model error function evaluated for the estimated optimal (minimum error) parameter combination [27,29]. To evaluate the sloppiness of our various candidate models the so called Levenberg-Marquardt approximation **L** of the Hessian, defined via [27,29]

$$L_{lm}(\theta^*) = \theta_l \theta_m \sum_{j=1}^{N_R} \frac{\partial r(t_j)}{\partial \theta_l} \frac{\partial r(t_j)}{\partial \theta_m} \big|_{\Theta = \Theta^*} \quad (23)$$

was used, where the derivatives were evaluated for the overall best parameter set $\Theta^* = (\theta_1^*, \theta_2^*, \ldots)$. Here $r(t_j)$ is the model firing rate at time t_j, and the sum goes over all N_R data points, in our case $201 \times 27 = 5427$. Note that the delay parameters Δ_{Ef} (and Δ_{If} for the models with feedforward inhibition) were left out of the analysis, since in our models the smallest possible step in this parameter was 0.5 ms. The depicted eigenvalues of **L** shown in Fig. 8 were normalized by the maximum eigenvalue.

The spectrum of these eigenvalues can be related to the shape of an ellipsoidal constant-error surface in a high-dimensional parameter space. The length of each principal axis of this constant-error surface is inversely proportional to the square root of the corresponding eigenvalue [27]. Directions with large eigenvalues are thus 'stiff' in the sense that the error increases rapidly in this direction. In contrast, in the 'sloppy' directions, corresponding to small eigenvalues, the error value changes little.

Thalamocortical model as differential equations

Derivation of differential equations. The full thalamocortical model on integral form in Eq. (1) can be mapped to a set of two differential equations by means of the 'linear chain trick' [5,14]. This model can be written as

$$r_4(t) = F_4(I_4(t)), \ I_4(t) = x_{E4}(t) - x_{I4}(t) + f_T(t) \quad (24)$$

where the auxiliary variables x_{E4}, x_{I4} and f_T are given by

$$x_{E4}(t) \equiv \beta_{Er}[h_{Er} * r_4](t), \quad (25)$$

$$x_{I4}(t) \equiv \beta_{Ir}[h_{Ir} * r_4](t), \quad (26)$$

$$f_T(t) \equiv \beta_{Ef}[h_{Ef} * r_T](t) - \beta_{If}[h_{If} * r_T](t) \quad (27)$$

Since the temporal coupling kernels all are given as exponentially decaying functions, differentiation of the expression for x_{E4} in Eq. (25) and x_{I4} in Eq. (26) with respect to time yields [14,76]

$$\frac{dx_{E4}}{dt} = \beta_{Er} \frac{d}{dt} \int_{-\infty}^{t} h_{Er}(t-s) F_4(I_4(s)) ds$$

$$= \frac{\beta_{Er}}{\tau_{Er}} F_4(I_4(t)) - \frac{\beta_{Er}}{\tau_{Er}} \int_{-\infty}^{t} h_{Er}(t-s) F_4(I_4(s)) ds \quad (28)$$

$$= \frac{\beta_{Er}}{\tau_{Er}} F_4(I_4(t)) - \frac{x_{E4}}{\tau_{Er}}$$

$$\frac{dx_{I4}}{dt} = \beta_{Ir} \frac{d}{dt} \int_{-\infty}^{t} h_{Ir}(t-s) F_4(I_4(s)) ds$$

$$= \frac{\beta_{Ir}}{\tau_{Ir}} F_4(I_4(t)) - \frac{\beta_{Ir}}{\tau_{Ir}} \int_{-\infty}^{t} h_{Ir}(t-s) F_4(I_4(s)) ds \quad (29)$$

$$= \frac{\beta_{Ir}}{\tau_{Ir}} F_4(I_4(t)) - \frac{x_{I4}}{\tau_{Ir}}$$

Here we have used that the delay constants Δ_{Er} and Δ_{Ir} in the recurrent coupling kernels $h_{Er}(t)$ and $h_{Ir}(t)$ are set to zero.

Stability analysis of thalamocortical model. On differential form the stability of the thalamocortical model can be directly assessed. For the situation with a stationary input f_{Ts}, the differential equation system in Eqs. (28–29) is given by

$$\frac{dx_{E4}}{dt} = -\frac{1}{\tau_{Er}} x_{E4} + \frac{\beta_{Er}}{\tau_{Er}} F_4(x_{E4} - x_{I4} + f_{Ts}), \quad (30)$$

$$\frac{dx_{I4}}{dt} = -\frac{1}{\tau_{Ir}} x_{I4} + \frac{\beta_{Ir}}{\tau_{Ir}} F_4(x_{E4} - x_{I4} + f_{Ts}) \quad (31)$$

The Jacobian of this autonomous equation system is given by

$$\mathbf{J} = \begin{bmatrix} \frac{1}{\tau_{Er}} \left(-1 + \beta_{Er} \frac{dF_4}{dI_4} \big|_{I_{4,eq}} \frac{dI_4}{dx_{E4}} \right) & \frac{\beta_{Er}}{\tau_{Er}} \frac{dF_4}{dI_4} \big|_{I_{4,eq}} \frac{dI_4}{dx_{I4}} \\ \frac{\beta_{Ir}}{\tau_{Ir}} \frac{dF_4}{dI_4} \big|_{I_{4,eq}} \frac{dI_4}{dx_{E4}} & \frac{1}{\tau_{Ir}} \left(-1 + \beta_{Ir} \frac{dF_4}{dI_4} \big|_{I_{4,eq}} \frac{dI_4}{dx_{I4}} \right) \end{bmatrix} \quad (32)$$

where $I_4 = x_{E4} - x_{I4} + f_{Ts}$. To ensure stability of the equilibrium point for this two-dimensional system, a negative trace $\text{tr}(\mathbf{J})$ and a positive determinant $\det(\mathbf{J})$ of the Jacobian is required (see, e.g., Wyller et al. [28]). For our activation function in Eq. (21) we have

$$\frac{dF_4}{dI_4} = \begin{cases} 0 & \text{if } I_4 < I_4^{\dagger} \\ a_4 & \text{if } I_4^{\dagger} \leq I_4 \leq I_4^* \\ a_4 + 2b_4(I_4 - I_4^*) & \text{if } I_4^* < I_4 \end{cases} \quad (33)$$

For the situation where the equilibrium point corresponds to I_4 on the linear flank of the activation function, we thus have $dF_4/dI_4 = a_4$ at the equilibrium value $I_{4,eq}$. We then find

$$\text{tr}(\mathbf{J}) = -\frac{1}{\tau_{Er}} + \frac{\beta_{Er}}{\tau_{Er}} a_4 - \frac{1}{\tau_{Ir}} - \frac{\beta_{Ir}}{\tau_{Ir}} a_4, \quad (34)$$

$$\det(\mathbf{J}) = \left(-\frac{1}{\tau_{Er}} + \frac{\beta_{Er}}{\tau_{Er}} a_4 \right) \left(-\frac{1}{\tau_{Ir}} - \frac{\beta_{Ir}}{\tau_{Ir}} a_4 \right) + \frac{\beta_{Er} \beta_{Ir}}{\tau_{Er} \tau_{Ir}} a_4^2$$

$$= \frac{1}{\tau_{Er} \tau_{Ir}} (1 - a_4(\beta_{Er} - \beta_{Ir})) \quad (35)$$

where we have used that $dI_4/dx_{E4} = 1$ and $dI_4/dx_{I4} = -1$. The requirements of a negative-trace and a positive-determinant for stability of the equilibrium point thus translate to the inequalities in Eqs. (6–7) in the main text.

These expressions can be directly generalized to the case where the background equilibrium state is on the parabolic part of the activation function by replacing a_4 by $a_4^* \equiv a_4 + 2b_4(I_{4,\mathrm{eq}} - I_4^*)$. Without recurrent excitation, i.e., $\beta_{\mathrm{Er}} = 0$, stability is always assured.

Thalamocortical transfer function

Our thalamocortical models are in general nonlinear due to the nonlinear activation function $F_4(I_4)$ described by Eq. (21). However, a linear transfer function can be found by linearization around a working point, i.e., by deriving the response to a small sinusoidal modulation $\tilde{r}_{\mathrm{T}}(\omega)$ in the thalamic input population firing rate superimposed on a constant background firing rate r_{T0}. Following a standard perturbative approach we make the ansatz

$$r_{\mathrm{T}}(t) = r_{\mathrm{T0}} + \tilde{r}_{\mathrm{T}}(\omega)e^{-i\omega t}, \tag{36}$$

$$r_4(t) = r_{40} + \tilde{r}_4(\omega)e^{-i\omega t} \tag{37}$$

With these expressions the convolutions in Eq. (1) can be rewritten as

$$[h * r](t) = \int_0^\infty h(s)r(t-s)ds = \int_0^\infty h(s)\left(r_0 + \tilde{r}(\omega)e^{-iw(t-s)}\right)ds \tag{38}$$
$$= \int_{-\infty}^\infty h(s)\left(r_0 + \tilde{r}(\omega)e^{-iw(t-s)}\right)ds = r_0 + \tilde{h}(\omega)\tilde{r}(\omega)e^{-iwt}$$

where we have used that (i) $h(t)$ is normalized, (ii) $h(t<0)=0$ by construction so that the lower boundary in the integral above can be set to $-\infty$, and (iii) introduced the Fourier transform $\tilde{h}(\omega) \equiv \int_{-\infty}^\infty h(s)\exp(iws)ds$. For our exponentially decaying coupling kernels in Eq. (20) we further find

$$\tilde{h}(\omega) = e^{i\omega\Delta}/(1 - i\tau\omega) \tag{39}$$

We now assume the perturbations in the input $\tilde{r}_{\mathrm{T}}(\omega)$ to be small and make the Taylor expansion

$$r_4(t) = F_4(I_4(t)) = F_4\left(I_{40} + \tilde{I}_4(\omega)e^{-i\omega t}\right)$$
$$\simeq F_4(I_{40}) + F_4'(I_{40})\tilde{I}_4(\omega)e^{-i\omega t} \tag{40}$$

so that we can identify $r_4(\omega) = F'(I_{40})\tilde{I}_4(\omega)$. By using the general mathematical result in Eq. (38) in the model expression Eq. (1) we thus find

$$\tilde{r}_4(\omega) = F_4'(I_{40})\tilde{I}_4(\omega) = \left(\beta_{\mathrm{Ef}}\tilde{h}_{\mathrm{Ef}}(\omega) - \beta_{\mathrm{If}}\tilde{h}_{\mathrm{If}}(\omega)\right)F_4'(I_{40})\tilde{r}_{\mathrm{T}}(\omega)$$
$$+ \left(\beta_{\mathrm{Er}}\tilde{h}_{\mathrm{Er}}(\omega) - \beta_{\mathrm{Ir}}\tilde{h}_{\mathrm{Ir}}(\omega)\right)F_4'(I_{40})\tilde{r}_4(\omega) \tag{41}$$

Algebraic rearrangement of this expression gives $\tilde{r}_4(\omega) = T_{4/\mathrm{T}}(\omega)\tilde{r}_{\mathrm{T}}(\omega)$ where $T_{4/\mathrm{T}}(\omega)$ is given by

$$T_{4/\mathrm{T}}(\omega) = \frac{F_4'(I_{40})\beta_{\mathrm{Ef}}\tilde{h}_{\mathrm{Ef}}(\omega) - F_4'(I_{40})\beta_{\mathrm{If}}\tilde{h}_{\mathrm{If}}(\omega)}{1 - F_4'(I_{40})\beta_{\mathrm{Er}}\tilde{h}_{\mathrm{Er}}(\omega) + F_4'(I_{40})\beta_{\mathrm{Ir}}\tilde{h}_{\mathrm{Ir}}(\omega)} \tag{42}$$

Reduction of two-population thalamocortical model

An alternative to the one-population Volterra model in Eq. (1) could be a generalization to a two-population Volterra model where both excitatory and inhibitory population firing rates are modeled explicitly. For the thalamocortical transformation this translates into including both an excitatory and an inhibitory layer-4 population, cf. Eqs. (14–15). With certain assumptions, however, this two-population model reduces to the one-population model in Eq. (1): with a *linear* inhibitory activation function, i.e., $F_{I4}(I_{I4}) = a_{I4}I_{I4}$, and no self-inhibition, i.e., $\alpha_{II} = 0$ [53], we find from Eqs. (14–15) that

$$I_{\mathrm{E4}} = \alpha_{\mathrm{TE}}h_{\mathrm{TE}} * r_{\mathrm{T}} - \alpha_{\mathrm{IE}}h_{\mathrm{IE}} * F_{I4}(I_{I4}) + \alpha_{\mathrm{EE}}h_{\mathrm{EE}} * r_{\mathrm{E4}}$$
$$= \alpha_{\mathrm{TE}}h_{\mathrm{TE}} * r_{\mathrm{T}} + \alpha_{\mathrm{EE}}h_{\mathrm{EE}} * r_{\mathrm{E4}} - \alpha_{\mathrm{IE}}h_{\mathrm{IE}} * F_{I4}(\alpha_{\mathrm{TI}}h_{\mathrm{TI}} * r_{\mathrm{T}} + \alpha_{\mathrm{EI}}h_{\mathrm{EI}} * r_{\mathrm{E4}}) \tag{43}$$
$$= (\alpha_{\mathrm{TE}}h_{\mathrm{TE}} - a_{I4}\alpha_{\mathrm{IE}}\alpha_{\mathrm{TI}}h_{\mathrm{IE}} * h_{\mathrm{TI}}) * r_{\mathrm{T}} + (\alpha_{\mathrm{EE}}h_{\mathrm{EE}} - a_{I4}\alpha_{\mathrm{IE}}\alpha_{\mathrm{EI}}h_{\mathrm{IE}} * h_{\mathrm{EI}}) * r_{\mathrm{E4}}$$

Then a term-by-term comparison shows that this expression has identical form as Eq. (1) provided the identifications

$$\alpha_{\mathrm{TE}}h_{\mathrm{TE}} \rightarrow \beta_{\mathrm{Ef}}h_{\mathrm{Ef}} \tag{44}$$

$$a_{I4}\alpha_{\mathrm{IE}}\alpha_{\mathrm{TI}}h_{\mathrm{IE}} * h_{\mathrm{TI}} \rightarrow \beta_{\mathrm{If}}h_{\mathrm{If}} \tag{45}$$

$$\alpha_{\mathrm{EE}}h_{\mathrm{EE}} \rightarrow \beta_{\mathrm{Er}}h_{\mathrm{Er}} \tag{46}$$

$$a_{I4}\alpha_{\mathrm{IE}}\alpha_{\mathrm{EI}}h_{\mathrm{IE}} * h_{\mathrm{EI}} \rightarrow \beta_{\mathrm{Ir}}h_{\mathrm{Ir}} \tag{47}$$

are made.

Author Contributions

Conceived and designed the experiments: AD IU GTE AMD. Performed the experiments: AD IU. Analyzed the data: PB UGI GTE AMD. Contributed reagents/materials/analysis tools: PB AD UGI GTE AMD. Wrote the paper: PB AD UGI IU GTE AMD.

References

1. Wilson HR, Cowan JD (1973) A mathematical theory of the functional dynamics of cortical and thalamic nervous tissue. Kybernetik 13: 55–80.

2. Amari S (1977) Dynamics of pattern formation in lateral-inhibition type neural fields. Biol Cybern 27: 77–87.

3. Deco G, Jirsa VK, Robinson PA, Breakspear M, Friston K (2008) The dynamic brain: From spiking neurons to neural masses and cortical fields. PLOS Comp Biol 4: e1000092. doi:10.1371/journal.pcbi.1000092.

4. Dayan P, Abbott LF (2001) Theoretical Neuroscience: Computational and Mathematical Modeling of Neural Systems. Cambridge MA: MIT Press.

5. Ermentrout B (1998) Neural networks as spatio-temporal pattern-forming systems. Rep Prog Phys 61: 353–430.

6. Coombes S (2005) Waves, bumps, and patterns in neural field theories. Biol Cybern 93: 91–108.

7. Kyriazi HT, Simons DJ (1993) Thalamocortical response transformations in simulated whisker barrels. J Neurosci 13: 1601–1615.

8. Pinto D, Brumberg JC, Simons JC, Ermentrout GB (1996) A quantitative population model of whisker barrels: Re-examining the Wilson-Cowan equations. J Comp Neuroscience 3: 247–264.

9. Pinto DJ, Hartings JA, Brumberg JC, Simons DJ (2003) Cortical damping: analysis of thalamocortical response transformations in rodent barrel cortex. Cereb Cort 13: 33–44.

10. Buzsaki G (2004) Large-scale recording of neuronal ensembles. Nat Neurosci 7: 446–451.

11. Einevoll GT, Pettersen KH, Devor A, Ulbert I, Halgren E, et al. (2007) Laminar Population Analysis: Estimating firing rates and evoked synaptic Activity from multielectrode recordings in rat barrel cortex. J Neurophysiol 97: 2174–2190.

12. Pettersen KH, Hagen E, Einevoll GT (2008) Estimation of population firing rates and current source densities from laminar electrode recordings. J Comp Neurosci 24: 291–313.

13. Pettersen KH, Einevoll GT (2008) Amplitude variability and extracellular low-pass filtering of neuronal spikes. Biophys J 94: 784–802.

14. Nordbø Ø, Wyller J, Einevoll GT (2007) Neural network firing-rate models on integral form: Effects of temporal coupling kernels on equilibrium-state stability. Biol Cybern 97: 195–209.

15. Pinto DJ, Brumberg JC, Simons DJ (2000) Circuit dynamics and coding strategies in rodent somatosensory cortex. J Neurophysiol 83: 1158–1166.

16. Wilent WB, Contreras D (2004) Synaptic responses to whisker deflections in rat barrel cortex as a function of cortical layer and stimulus intensity. J Neurosci 24: 3985–3998.

17. Blomquist P, Indahl UG, Devor A, Ulbert I, Einevoll GT, et al. (2006) Estimation of cortical microcircuit model from joint thalamic single-unit and cortical laminar-electrode recordings in rat whisker-barrel system. Soc Neurosci Abstr 53: 23.

18. Kyriazi HT, Carvell GE, Simons DJ (1994) OFF response transformations in the whisker/barrel system. J Neurophysiol 72: 392–401.

19. Beierlein M, Fall CP, Rinzel J, Yuste R (2002) Thalamocortical bursts trigger recurrent activity in neocortical networks: layer 4 as a frequency-dependent gate. J Neurosci 22: 9885–9894.

20. Feldmeyer D, Egger V, Lübke J, Sakmann B (1999) Reliable synaptic connections between pairs of excitatory layer 4 neurones within a single "barrel" of developing rat somatosensory cortex. J Physiol 521: 169–190.

21. Beierlein M, Gibson JR, Connors BW (2003) Two dynamically distinct inhibitory networks in layer 4 of the neocortex. J Neurophysiol 90: 2987–3000.

22. Swadlow HA, Gusev AG (2002) Receptive-field construction in cortical inhibitory interneurons. Nature Neurosci 5: 403–404.

23. Swadlow HA (2003) Fast-spike interneurons and feedforward inhibition in awake sensory neocortex. Cereb Cort 13: 25–32.

24. Sun Q-Q, Huguenard JR, Prince DA (2006) Barrel cortex microcircuits: thalamocortical feedforward inhibition in spiny stellate cells is mediated by a small number of fast-spiking interneurons. J Neurosci 26: 1219–1230.

25. Temereanca S, Simons DJ (2004) Functional topography of corticothalamic feedback enhances thalamic spatial response tuning in the somatosensory whisker/barrel system. Neuron 41: 639–651.

26. Tateno T, Harsch A, Robinson HPC (2004) Threshold firing frequency-current relationships of neurons in rat somatosensory cortex: Type 1 and type 2 dynamics. J Neurophysiol 92: 2283–2294.

27. Gutenkunst RN, Waterfall JJ, Casey FP, Brown KS, Myers CR, et al. (2007) Universally sloppy parameter sensitivities in systems biology models. PLoS Comp Biol 3: 1871–1878. doi:10.1371/journal.pcbi.0030189.

28. Wyller J, Blomquist P, Einevoll GT (2007) Turing instability and pattern formation in a two-population neuronal network model. Physica D 225: 75–93.

29. Brown KS, Sethna JP (2003) Statistical mechanical approaches to models with many poorly known parameters. Phys Rev E 68: 021904.

30. Oppenheim AW, Willsky AS (1996) Signals&Systems. 2nd ed. Upper Saddle River, New Jersey: Prentice.

31. Bracewell RN (1999) The Fourier transform and its applications. 3rd ed. Columbus, Ohio: McGraw-Hill.

32. Einevoll GT, Plesser HE (2002) Linear mechanistic models for the dorsal lateral geniculate nucleus of cat probed using drifting-grating stimuli. Network: Comp Neur Syst 13: 503–530.

33. Webber RM, Stanley GB (2004) Nonlinear encoding of tactile patterns in the barrel cortex. J Neurophysiol 91: 2010–2022.

34. Petersen CCH, Sakmann B (2001) Functionally independent columns of rat somatosensory barrel cortex revealed with voltage-sensitive dye imaging. J Neurosci 21: 8435–8446.

35. Feldmeyer D, Lübke J, Silver RA, Sakmann B (2002) Synaptic connections between layer 4 spiny neurone - layer 2/3 pyramidal cell pairs in juvenile rat barrel cortex: physiology and anatomy of interlaminar signalling within a cortical column. J Physiol 538.3: 803–822.

36. Lübke J, Roth A, Feldmeyer D, Sakmann B (2003) Morphometric analysis of the columnar innervation domain of neurons connection layer 4 and layer 2/3 of juvenile rat barrel cortex. Cereb Cort 13: 1051–1063.

37. Thomson AM, Bannister AP (2003) Interlaminar connections in the neocortex. Cereb Cort 13: 5–14.

38. Helmstaedter M, de Kock CPJ, Feldmeyer D, Bruno RM, Sakmann B (2007) Reconstruction of an average cortical column in silico. Brain Res Rev 55: 193–203.

39. Lübke J, Feldmeyer D (2007) Excitatory signal flow and connectivity in a cortical column: focus on barrel cortex. Brain Struct Funct 212: 3–17.

40. Sarid L, Bruno R, Sakmann B, Segev I, Feldmeyer D (2007) Modeling a layer 4-to-layer 2/3 module of a singe column in rat neocortex: Interweaving in vitro and in vivo experimental observations. Proc Natl Acac Sci U S A 41: 16353–16358.

41. Thomson AM, Lamy C (2007) Functional maps in neocortical local circuitry. Front in Neurosci 1: 19–42.

42. Feldmeyer D, Lübke J, Sakmann B (2006) Efficacy and connectivity of intracolumnar pairs of layer 2/3 pyramidal cells in the barrel cortex of juvenile rats. J Physiol 575.2: 583–602.

43. Feldmeyer D, Roth A, Sakmann B (2005) Monosynaptic connections between pairs of spiny stellate cells in layer 4 and pyramidal cells in layer 5A indicate that lemniscal and paralemniscal afferent pathways converge in the infragranular somatosensory cortex. J Neurosci 25: 3423–3431.

44. Schubert D, Kötter R, Luhmann HJ, Staiger JF (2006) Morphology, electrophysiology and functional input connectivity of pyramidal neurons characterizes a genuine layer Va in the primary somatosensory cortex. Cereb Cort 16: 223–236.

45. Bruno RM, Sakmann B (2006) Cortex is driven by weak and synchronously active thalamocortical synapses. Science 312: 1622–1627.

46. de Kock CPJ, Bruno RM, Spors H, Sakmann B (2007) Layer- and cell-type specific suprathreshold stimulus representation in rat primary sensory cortex. J Physiol 581: 139–154.

47. Shepherd GMG, Svoboda K (2005) Laminar and columnar organization of ascending excitatory projections to layer 2/3 pyramidal neurons in rat barrel cortex. J Neurosci 25: 5670–5679.

48. Schroeder CE, Lindsley RW, Specht C, Marcovici A, Smiley JF, Javitt DC (2001) Somatosensory input to auditory association cortex in the macaque monkey. J Neurophysiol 85: 1322–1327.

49. Ulbert I, Halgren E, Heit G, Karmos G (2001) Multiple microelectrode-recording system for human intracortical applications. J Neurosci Meth 106: 69–79.

50. Covert RF, Scheriber MD, Leff AR, White SR, Munoz NM, et al. (1992) Oxygen metabolism and catecholamine secretion during chloralose anesthesia in lambs. J Dev Physiol 17: 125–132.

51. Lindauer U, Villringer A, Dirnagl U (1993) Characterization of CBF response to somatosensory stimulation: model and influence of anesthetics. Am J Physiol 264: H1223–1228.

52. Ueki M, Mies G, Hossmann KA (1992) Effect of alpha-chloralose, halothane, pentobarbital and nitrous oxide anesthesia on metabolic coupling in somato-sensory cortex of rat. Acta Anaesthesiol Scand 36: 318–322.

53. Pinto D, Ermentrout B (2001) Spatially structured activity in synaptically coupled neuronal networks: II Lateral inhibition and standing pulses. SIAM J Appl Math 62: 226–243.

54. Shriki O, Hansel D, Sompolinsky H (2003) Rate models for conductance-based cortical neuronal networks. Neural Comp 15: 1809–1841.

55. Kriener B, Tetzlaff T, Aertsen A, Diesmann M, Rotter S (2008) Correlations and population dynamics in cortical networks. Neural Comp 20: 2133–2184.

56. Petreanu L, Huber D, Sobczyk A, Svoboda K (2007) Channelrhodopsin-2-assisted circuit mapping of long-range callosal projections. Nat Neurosci 10: 663–668.

57. Wise SP, Jones EG (1976) The organization and postnatal development of the commissural projection of the rat somatic sensory cortex. J Comp Neurol 168: 313–343.

58. White EL, DeAmicis RA (1977) Afferent and efferent projections of the region in mouse SmL cortex which contains the posteromedial barrel subfield. J Comp Neurol 175: 455–482.

59. Koralek KA, Olavarria J, Killackey HP (1990) Areal and laminar organization of corticocortical projections in the rat somatosensory cortex. J Comp Neurol 299: 133–150.

60. Li L, Ebner FF (2006) Balancing bilateral sensory activity: callosal processing modulates sensory transmission through the contralateral thalamus by altering the response threshold. Exp Brain Res 172: 397–415.

61. Vogt BA, Gorman AL (1982) Responses of cortical neurons to stimulation of corpus callosum in vitro. J Neurophysiol 48: 1257–1273.

62. Olavarria J, Van Sluyters RC, Killackey HP (1984) Evidence for the complementary organization of callosal and thalamic connections within rat somatosensory cortex. Brain Res 291: 364–368.

63. Derdikman D, Hildesheim R, Ahissar E, Arieli A, Grinvald A (2003) Imaging spatiotemporal dynamics of surround inhibition in the barrels somatosensory cortex. J Neurosci 23: 3100–3105.

64. Devor A, Tian P, Nishimura N, Teng IC, Hillman EM, et al. (2007) Suppressed neuronal activity and concurrent arteriolar vasoconstriction may explain negative blood oxygenation level-dependent signal. J Neurosci 27: 4452–4459.
65. Hlushchuk Y, Hari R (2006) Transient suppression of ipsilateral primary somatosensory cortex during tactile finger stimulation. J Neurosci 26: 5819–5824.
66. Ferbert A, Priori A, Rothwell JC, Day BL, Colebatch JG, et al. (1992) Interhemispheric inhibition of the human motor cortex. J Physiol 453: 525–546.
67. Ogawa S, Lee TM, Stepniski R, Chen W, Zhu XH, et al. (2000) An approach to probe some neural systems interaction by functional MRI at neural time scale down to milliseconds. Proc Natl Acad Sci U S A 97: 11026–11031.
68. Horwitz B, Tagamets MA, McIntosh AR (1999) Neural modeling, functional brain imaging, and cognition. Trends Cogn Sci 3: 91–98.
69. Buchel C, Friston KJ (2000) Assessing interactions among neuronal systems using functional neuroimaging. Neural Networks 13: 871–882 2000.
70. Friston KJ (2005) A theory of cortical responses. Philos Trans R Soc Lond B Biol Sci 360: 815–836.
71. Friston K (2008) Hierarchical models in the brain. PLOS Comp Biol 4: e1000211. doi:10.1371/journal.pcbi.1000211.
72. Dale AM, Sereno MI (1993) Improved localization of cortical activity by combining EEG and MEG with MRI cortical surface reconstruction: a linear approach. J Cog Neurosci 5: 162–176.
73. Dale AM, Halgren E (2001) Spatiotemporal mapping of brain activity by integration of multiple imaging modalities. Curr Opin Neurobiol 11: 202–208.
74. Ahissar E, Sosnik R, Baqdasarian K, Haidarliu S (2001) Temporal frequency of whisker movement. II. Laminar organization of cortical representations. J Neurophysiol 86: 354–367.
75. Dale AM (1999) Optimal experimental design of event-related fMRI. Hum Brain Map 8: 109–114.
76. Cushing JM (1977) Integrodifferential equations and delay models in population dynamics, lecture notes in biomathematics. Heidelberg: Springer.